Studies on the Fluidized Snow Dynamics

by

Kouichi Nishimura
西 村 浩 一
The Institute of Low Temperature Science

Received January 1991

Abstract

An inclined chute system and a fluidized snow bed were constructed in a cold laboratory and extensive measurements of mechanical properties of fluidized snow were carried out. In the steady part of the snow flow, where the thickness and velocities are roughly constant, velocity profiles were obtained at various chute inclinations. Assuming that the bulk densities are uniform with depth, a constitutive equation of a Bingham body was applied to simulate the obtained velocity profiles. The apparent viscosity coefficients obtained ranged from 8.3×10^{-2} to 4.5×10^{-1} Ns/m^2 and yield stress 0 to 10 N/m^2 for the bulk densities of 100 to 200 kg/m^3 and the shear rate of 60 to 70 s^{-1}. On the other hand viscous properties of the fluidized snow which was produced with the fluidized-bed experiment system was investigated with the Brookfield viscometer. All sets of data showed that the relation between the shear stress and shear rate satisfied the constitutive equation of the Bingham body for the shear rate of 1 to 15 s^{-1}. Viscosity coefficients of the fluidized snow obtained ranged from 10^{-2} to 10^{-1} Ns/m^2; yield stress were 0 to 10^{-2} N/m^2. It was also found that the viscosity increased rapidly with the bulk density.

The viscosity coefficients obtained in the two different systems were compared in special reference to the shear rate of each experiment; The assumptions made in the former calculations were re-examined. Consequently it was revealed that shear stresses are linearly proportional to the shear rate in a lower shear rate region and shear stresses depend on the square of the shear rate in a higher shear rate region. Furthermore a constitutive equation which expresses the general dynamical properties of fluidized snow was found to be written as the sum of the dry friction, the viscous and the quadratic viscous terms.

The dynamical properties of the fluidized snow obtained in the above experiments and analyses were applied to the numerical simulations of the fluidized snow flow motion along the chute and artificial and natural avalanches observed in the Shiai-dani region, showing a reasonable fit of the observed data.

* Contribution No. 3441 from the Institute of Low Temperature Science
北海道大学審査学位論文

Contents

I. Introduction

Fluidized snow is defined as a mixture of snow particles and air in which both of them are in motion. Avalanches and blowing snow are its typical examples often observed in nature. In snow engineering fields dispersing snow particles thrown away from rotary snow removal machines are familiar; Recently pneumatic convey of snow in transport pipes as well as hydraulic transport with gutters have attracted special interest. Understanding of physical properties of fluidized snow should be very helpful not only to scientists who study the mechanism and dynamics of avalanches and drifting snow, but also to engineers who are engaged in improving the efficiency of snow transport system. However so far little systematic work has been done on the physical properties of fluidized snow.

We constructed a chute experimental system and a fluidized snow bed in a cold laboratory and carried out extensive measurements of mechanical properties of fluidized snow. In this paper results of those experiments are presented to give insight into the mechanism of momentum transport processes in fluidized snow. Chapter II reviews previous works carried out so far to understand the physical properties of fluidized snow; Chapter III gives results of inclined chute experiments of snow flows, Chapter IV gives results of fluidized-bed experiments of snow. In Chapter V we compare the results of both the experiments and propose a constitutive equation which expresses the general dynamical properties of fluidized snow, in Chapter VI we show numerical simulations of avalanche motion by applying the obtained dynamical properties of fluidized snow, and finally in Chapter VII we summarize the conclusive results of the present work and give the future scope.

II. Previous works

The general behavior of fluidized snow has been recognized to be similar to those of a fluid. It is well known that snow avalanches behave like viscous fluids and flow rapidly on slopes and around obstacles. Kobayashi(1978) even suggested that transverse snow-waves formed during the drifting snow over the snow surface possibly caused by the surface waves of the liquid-like fluidized snow.

By the analogy between motions of snow particles in fluidized snow and molecules in a liquid, it is expected that momentum transport processes are rapid and effective in fluidized snow. But there is not enough basic data; Maeno and Nishimura(1978) and Nishimura and Maeno(1978) have studied experimentally the fluidization of snow in a cold laboratory. They found that the value of viscosity coefficient in a fully fluidized snow were comparable to that of water(1×10^{-3} Ns/m^2). Lang and Dent (1983) dragged sleds coated with sand over hard sintered snow and found the viscosity coefficient of a thin fluidized layer ranges from 0.2 to 1.0 Ns/m^2. Casassa (1989) investigated the friction between snow and snow. He slid

down blocks of hard sintered snow on the natural snow slopes and obtained the value of viscosity of fluidized snow formed between surfaces as 6.6×10^{-2} to 4.8×10^{-1} Ns/m^2.

Furthermore obtained values showed scatters in a wide range: values reported by Maeno and Nishimura(1978) are by two to three orders of magnitude smaller than those by Dent and Lang(1983). Physical relations between viscosity coefficients and bulk snow densities have not been derived nor understood well.

III. Inclined chute experiments of snow flows

III.1. *Experimental apparatus and procedures*

A photograph and a schematic diagram of the experimental setup are shown in Fig. 1 and Fig. 2 respectively. The main apparatus consists of two parts: fluidized snow feeder and inclined chute. Fig. 3 is the picture of the fluidized snow feeder which has a cylindrical basin 90 cm in inner diameter and 30 cm in height. The center shaft with three rotors rotates about one r.p.s. in the basin; about 10 kg in weight of snow can be kept in disintegrated and fluidized condition.

Generally the snow, 5 to 7 kg in weight, was supplied to an inclined chute within a period of 1-2 s from the fluidized snow feeder. The chute was 5.4 m long and 0.08 m wide, as shown in Fig. 2. The angle of inclination could be varied between 30° and 45°. The floor of the chute was covered with sandpaper, sintered (packed) snow or polyetylene film. The whole

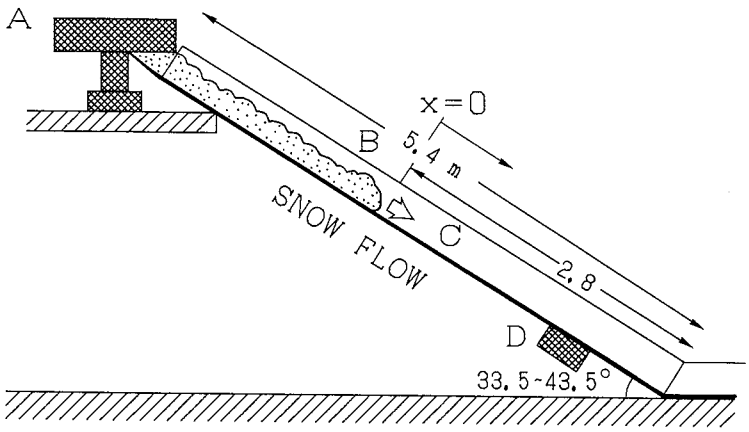

Fig. 1 Schematic diagram showing the experimental set-up.
A: fluidized snow feeder,
B: chute,
C: sand paper or snow,
D: drag meter.

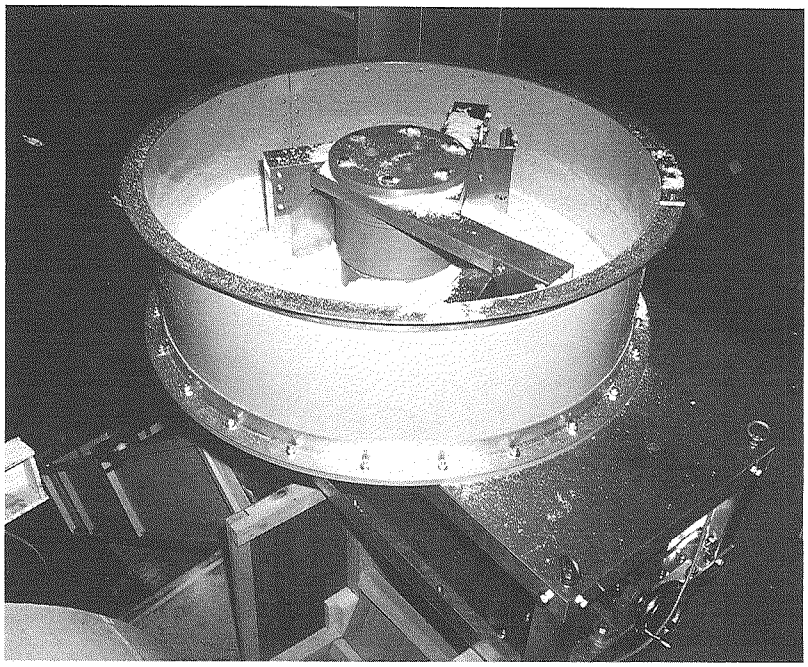

Fig. 2 Photograph of the fluidized snow feeder.

experiment system was installed in a cold room and all the measurements were carried out at a temperature of −15 ℃. The temperature was chosen to avoid the complex effect of adhesion between snow particles.

The movement of individual snow particles and the snow flow height were viewed and recorded from a side of the chute, with a high-speed video system (NAC, HSV-200) taking 200 frames per second.

A drag meter was newly designed and set on the chute floor at the position of $x=160$ cm, where x is measured from the point (0) in Fig. 2 along the chute; The point 0 is 2.6 m downward from the chute entrance, where the snow flow becomes roughly steady as shown later in detail. A schematic diagram of the drag meter is shown in Fig. 4 and its picture in Fig. 5. The drag plate had a size of 13 cm×6 cm and the surface was covered with sand paper. It can move freely through frictionless ball-bearings against the framework. Thus the shear stress acting on the drag plate could be measured with the strain-gauge-type load -cell (KYOWA, LU5KA) installed on the framework.

In some runs bulk densities in a flow were monitored by an electric capacitance measurement; Electric capacitance of a flow volume, 20 mm×50 mm×5 mm, was measured at two levels (10 mm and 35 mm above the floor) by using capacitance-meters operating at 3.5 MHz (Iwatsu, ST3501). Details of the measuring technique are given in Maeno(1986).

Measured values of electric capacitance can be converted to bulk snow densities, but in this paper the measured capacitance values were used to estimate the relative density variation.

Pictures obtained with the high speed video system were analyzed with the X-Y coordinator (NAC, V-10) and a microcomputer system (NEC, PC-9801). Data of bulk densities and shear stress were recorded simultaneously on an analog cassette data recorder (TEAC, R-61). Then they were transformed into digital values using an A-D converter (Microscience, DAS-1898BPC) and analyzed with a microcomputer system. The shear stress measured had big noises to signals due to inherent vibrations of the total system, the frequency of which was about 20 Hz. Thus a low-pass filter having a cutoff frequency of 17.5 Hz was applied. These procedures are shown schematically in Fig. 6; In this way the following four independent variables were obtained in each experiment: snow flow thickness, snow particle velocities, bulk density, and shear stress (drag force) acting on the chute floor.

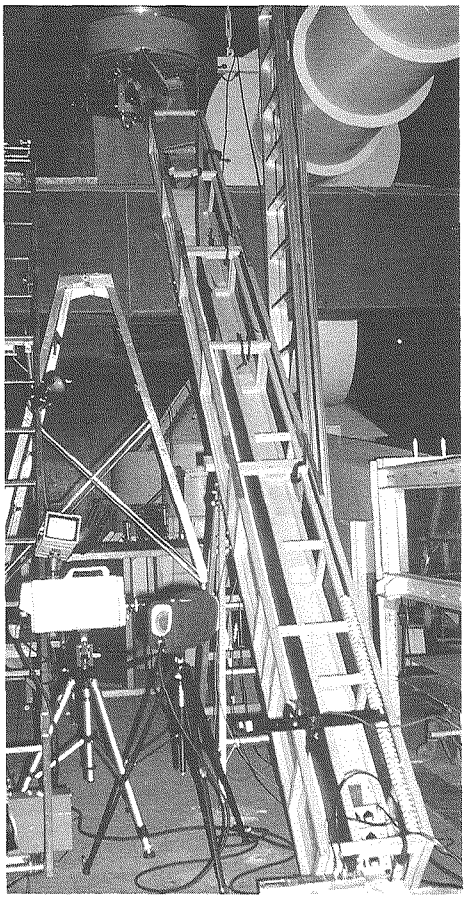

Fig. 3 General view of the experimental set-up.

III.2. *Snow samples*

The snow used in the experiments was natural fine-grained snow, which was collected from the suburbs of Sapporo city and kept in a cold room at −10 °C for about ten months before use. Fig. 7 gives histograms of particle sizes of samples. Particle sizes are expressed as diameters of circles with equivalent projected areas, which were measured from microphotographs containing 20-50 particles. The size distributions can roughly be regarded as normal distribution. The average diameter of the fine-grained snow particles was 0.59 mm.

The angle of repose of the snow observed in a cold laboratory at −15 °C was 31.3° on average with 5° of standard deviation.

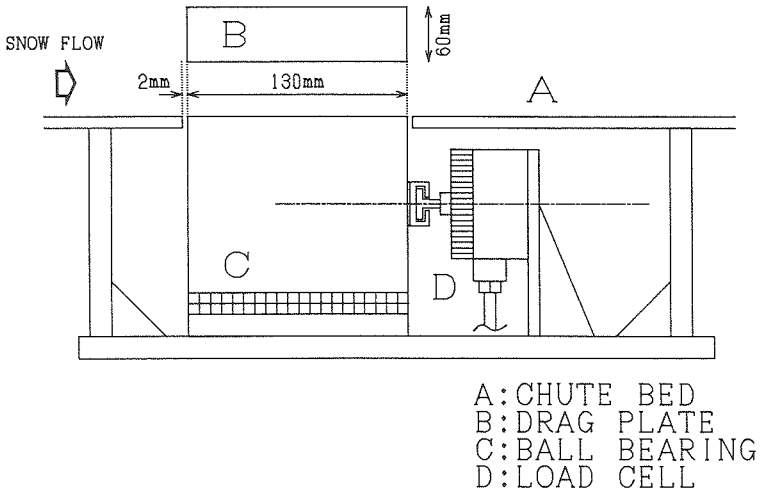

Fig. 4 Fundamentals of the drag meter's structure.

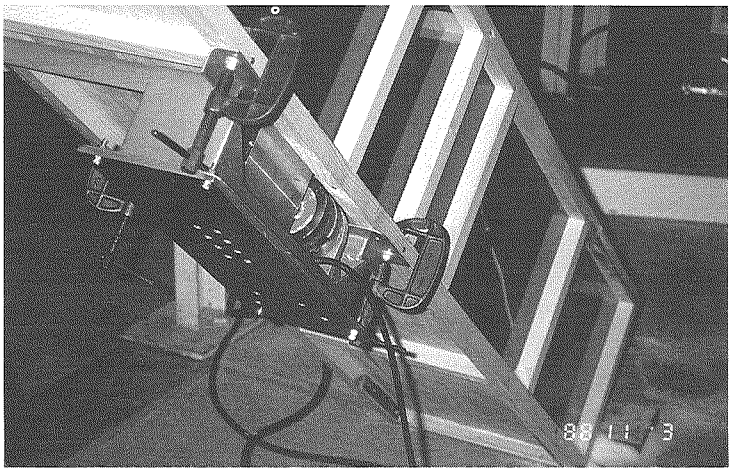

Fig. 5 Photograph of the drag meter mounted on the chute bed.

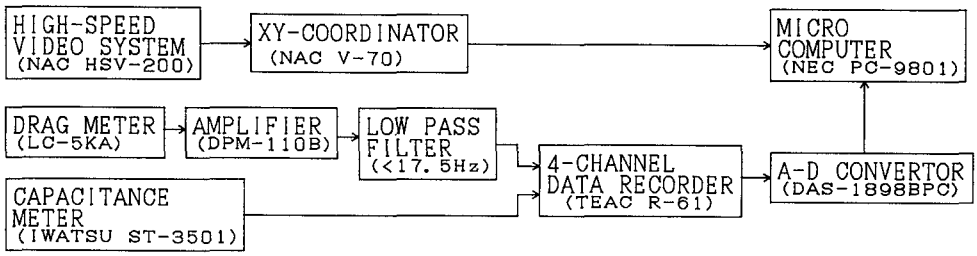

Fig. 6 Block diagram of the measuring and analyzing system.

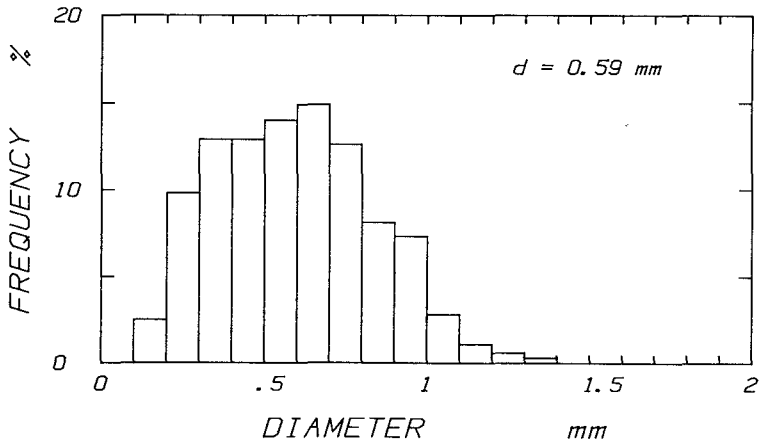

Fig. 7 Histogram of snow particle diameters.

III.3. *Results and analyses*

Figs. 8 (a) and (b) are pictures of a snow flow taken by a high speed video system. Fig. 8 (a) shows the following: the front region of a snow flow is about 4 cm thickness and the density is not so high that the wooden wall can be seen through. Fig. 8 (b) is the picture of snow flow which comes after the front region and seems to keep roughly a constant thickness. It is clear from this picture that the snow flow consists of two layers, namely the upper snow-dust and lower flowing layers. Further these two layers are distinguished clearly by an interface. As can be seen in this figure, the bulk density in the snow-dust layer is quite low, but is rather high in the flowing layer. In this paper we are only concerned with the flowing layer, which occupies the majority of a snow flow mass. The maximum height of the flowing layer in each experiment was roughly 4 to 6 cm.

a) Velocities of snow particles

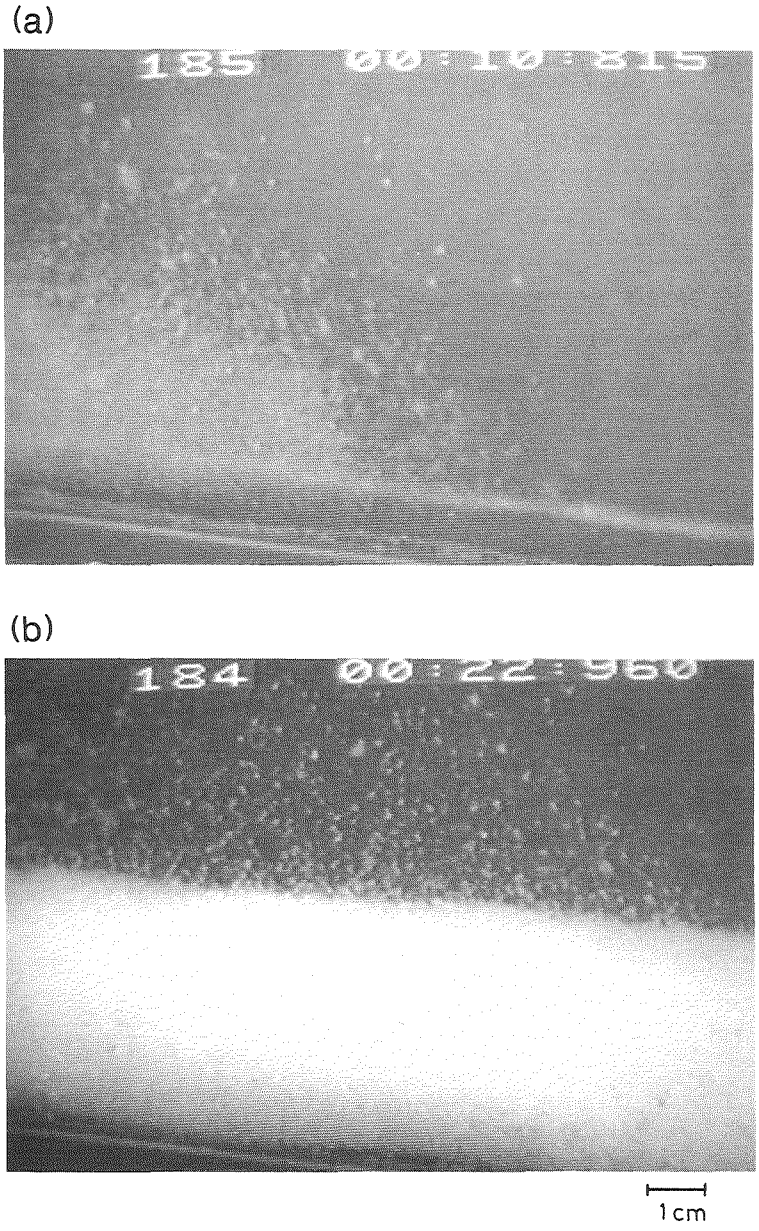

Fig. 8 Photographs of the fluidized snow flow.
(a): front region, (b): center region.

Fig. 9 shows the surface velocity profiles across a snow flow, which were measured at $x=2.0$ m, 2.3 m and 2.7 m. Effects of wall-friction are noted at both the sides (one wall, $z=0$ cm is glass and the other, $z=8$ cm, wood); but they are usually small, less than 10% of the center velocity. Hereafter many velocities of snow particles are presented and discussed, which correspond to those measured from the side of the chute, namely at $z=0$.

Fig. 10 shows the typical velocity profiles of individual snow particles obtained under different boundary conditions: polyethylene film, sand paper and snow. Each datum shown is the average of several snow samples within 2 mm thickness. It is a purpose of the experiment to create the fluidized snow flow over the snow surface like an avalanche in nature. As shown in Fig. 10 velocity profile is almost non-slip on the snow surface and velocity attains 5 m/s at a height of 5 cm. But the snow surface experiment has some technical problems: it is so hard to prepare a snow surface reproducibly and to set the instruments (drag meter, electrodes) in the chute. Thus sand paper (#30) which is easier to handle was mostly used in place of snow. It was glued hard particles 420 to 710 μm in diameter; the particle size is equivalent to that of snow particles used in this experiment. It is evident in Fig. 10 that sand paper floor creates almost the similar flow to that on the snow floor. However polyethylene film was also tried as a chute floor to achieve high velocities. A larger slip velocity above 3.5 m/s was found and velocity shear became smaller. As large shear and no-slip conditions are more attractive and practical to investigate the physical properties of fluidized snow, in

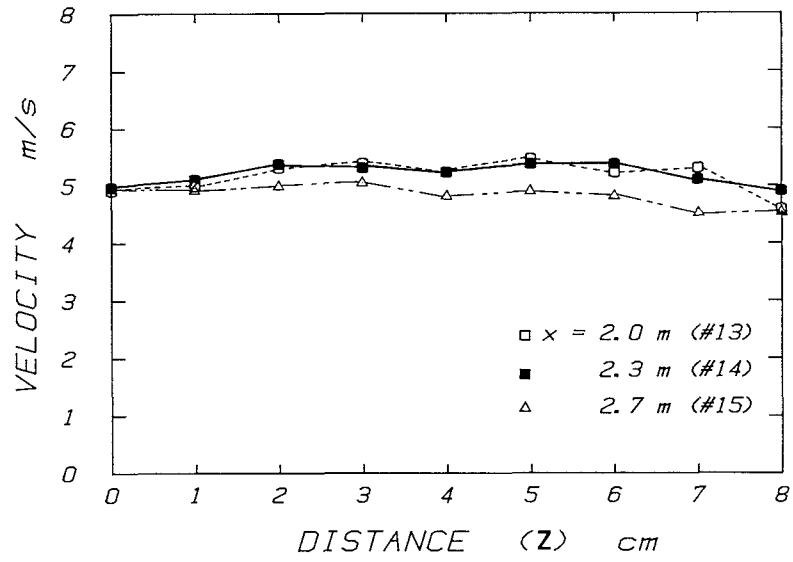

Fig. 9 Velocity profiles across a snow flow.
Measured at $x=2.0$, 2.3 and 2.7 m.
Walls are glass ($z=0$) or wood ($z=8$).

the following we will mainly discuss the experiments carried out on the sand paper.

Generally fluidized snow supplied from the feeder for about a second produced a flow of 4 to 5 cm thick and 6 m long at $x=0$. Fig. 11 shows the typical example of the time variation of a snow flow thickness observed at a fixed position ($x=180$cm). The depth of the snow flow was found to range from 10 mm to 60 mm. Though there are slight changes in the snow

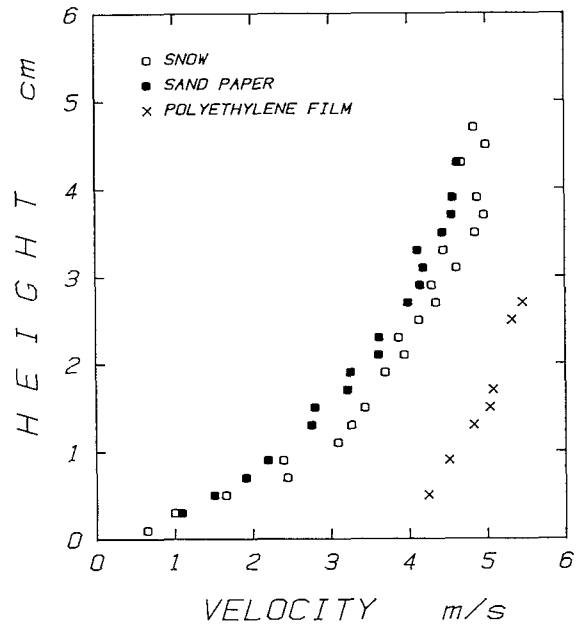

Fig. 10 Velocity profiles of the snow flow on various floor conditions.

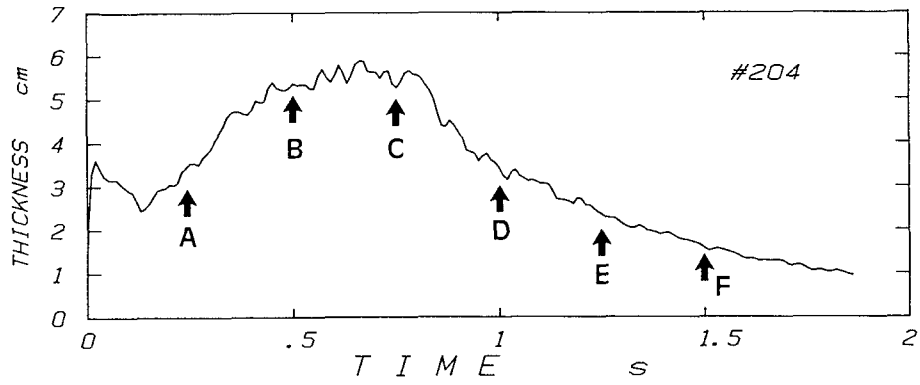

Fig. 11 Variation in snow flow depth with time.

flow thickness due mainly to the mechanism of the fluidized snow-feeder, the overall profile was considerably reproducible. After the passage of the front region in which thickness is rather high and density is low as shown in Fig. 7, the snow flow thickness increased. At 0.5 s on Fig. 11 it reached a maximum and remained roughly constant or fluctuated around the mean for 0.5 s. In the following 1 s to 1.5 s it became thinner gradually. Fig. 11 shows six points A, B, C, D, E and F, which are chosen every 0.25 s. A corresponds to a region near the front; B and C to regions in which the thickness was roughly constant; D, E and F to a region in which the thickness decreased gradually.

Velocity profiles of the flow at each point is shown in Fig. 12. It is evident from this figure that velocity profiles of B and C resemble each other, moreover maximum velocities of B and C are larger than those of front (A) and rear parts (D, E, F); That is, the region where the thickness remained roughly constant shows not only constant but also highest velocity in the snow flow. Thus it can be concluded that it is the steady-state part of the fluidized snow flow. Considering from the time of passage in Fig. 11 and the flow velocity in Fig. 12, the steady-state part is estimated about 2 m long and 4-5 cm thick.

Fig. 13 shows the change in the velocity of the steady-state part over the chute. Each datum, shown in Fig. 13, was obtained for different runs, but each of the total amounts of snow flow was almost comparable. Though the velocity increases slightly from $x=0$ cm to the chute exit ($x=260$ cm), it seems to be reasonable to consider that the snow flow velocity has attained a steady state. Besides Fig. 13 shows that both the snow and sand-paper floors are equivalent in the velocity change along the chute as well as in the velocity profiles shown in Fig. 10.

Fig. 14 shows the steady state velocity profile of a snow flow at various chute-inclinations. For inclinations of 43.5°, 41.5°, and 37.5°, a velocity gradient was found over the depth of snow flow. While at 33.5°, snow flow consists of two layers; in the upper layer snow particles move like a rigid body and in the lower layer a strong velocity gradient, that is shear, exists. A similar result was obtained when new snow flowed over a packed snow surface in the field (Nishimura & Maeno, 1989). Ishida et al. (1980) observed five types of flow patterns in experiments of granular chute flows that were fluidized by an upward air flow along the channel bed. With zero fluidization-air-flow they observed three types of granular flows: immature sliding flow, sliding flow, and splashing flow. The first occurred when the bed inclination is close to the angle of repose and velocity profile has a concave shape. With a small increase in bed inclination, sliding flow occurred, which has a triangular velocity profile. Further increase in bed slope leads to a splashing flow which has a blunt velocity profile with a higher shear rate near the bed than near the upper surfaces. As the angle of repose of our snow was 31.5°, the experiments of 43.5° and 41.5° are considered to belong to the splashing flow regime. In fact a blunt profile was observed in those experiments. Further in the experiment of 37.5° triangular profile can be seen. But in the experiment of 33.5°, considered to be a sliding flow, the concave velocity profile was not

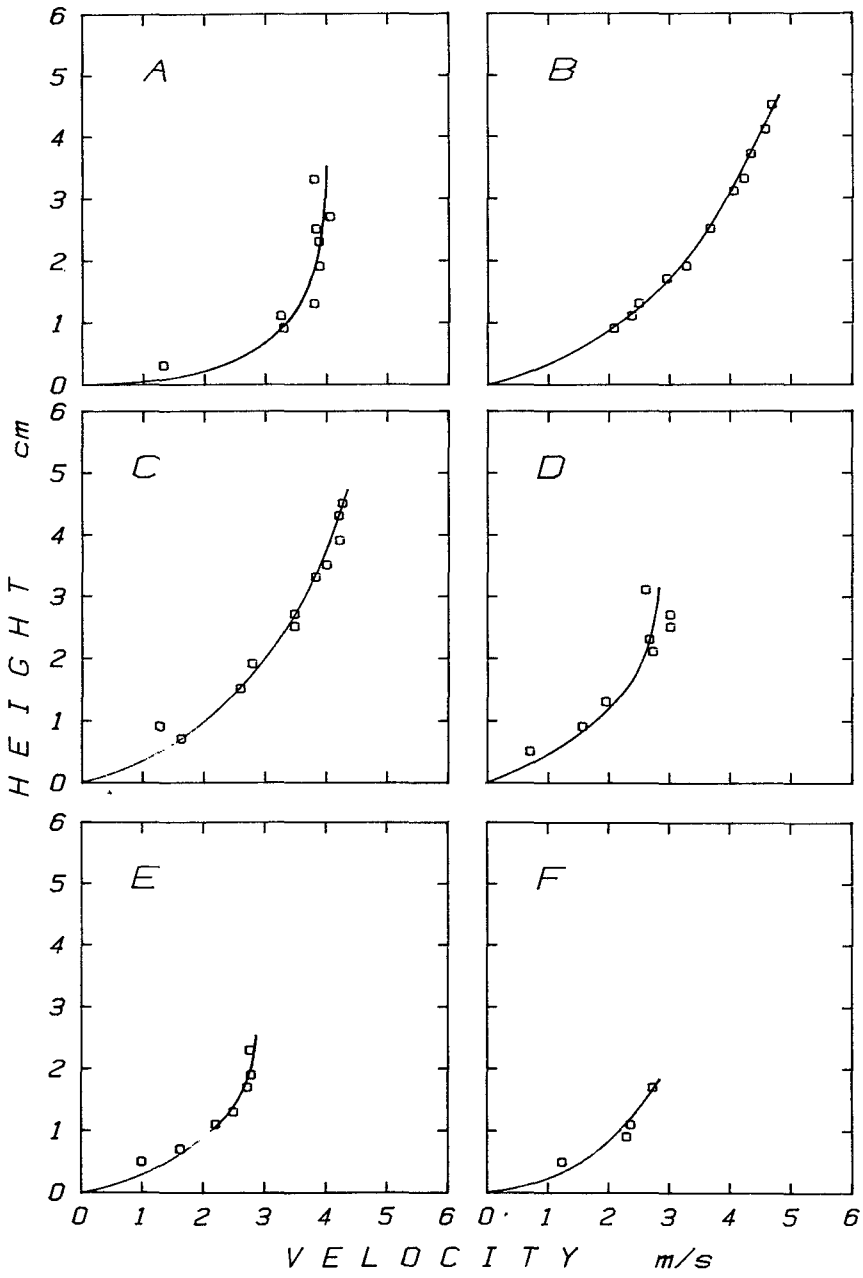

Fig. 12 Velocity profiles of the snow flow at A, B, C and D in Fig. 11.

found.

Measured snow velocity of steady-state part may include effects of surface air drag (F_a) acting on the upper surface (area: S_s, a drag coefficient: C_s). Thus:

$$F_a = 0.5 C_s S_s \rho_a v^2 \qquad (1)$$

where v is the velocity of the snow flow and ρ_a is the air density (1.3 kg/m^3). The highest velocity for our runs was 5 m/s. Putting the kinematic viscosity of air (ν_a) to be 1.47×10^{-5} m^2/s and a characteristic dimension of a stead-state snow flow to be 2 m, the Reynolds number (Re) was calculated as $Re=6.8\times10^5$. Standard values of C_s for this order of Re are smaller than 0.01 (Prandtl, 1965). Adopting these upper limits, the air drag for a velocity of 5 m/s amounts to $F_a=0.026$ N/m^2 ($S_s=2$ m$\times$0.08 m), which is about 0.08 % of the basal shear stress acting on the bed (about 30 N/m^2, see Fig.34). Thus the effect of the air drag can be ignored.

Fig. 15 shows the relation between maximum velocities obtained from steady state velocity profiles and chute angles. Fluidized snow particles are considered to begin to flow down the chute when the inclination becomes slightly larger than the angle of repose. Thus it is clear that snow flow velocity increases rapidly with inclination angle at first and much less for the inclination larger than 37.5°. This tendency was also found in the sand flow investigated by Takahashi(1937). He studied the velocity of sand particles (estimated from their trajectories) leaving the downstream end of the chute (150 cm long and a few centi-

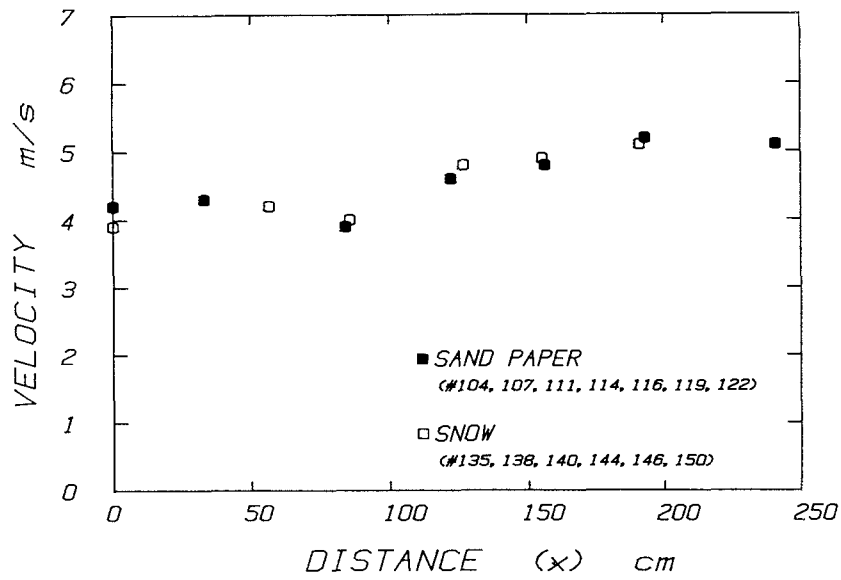

Fig. 13 Change in the snow flow velocity over the inclined chute.

meters wide). Two kinds of modes, which are equivalent to those shown in Fig.15, were found in the sand flow and the analogy with the laminar and turbulent flows in hydrodynamics were discussed.

b) Bulk densities of snow flows

The bulk density of a snow flow is difficult to measure precisely by direct sampling. Furthermore low transmissivity of light in the flowing layer eliminates possibility of some conventional optical measurements. In order to overcome this difficulty a new and simpler method of measuring the bulk density was developed by using the drag meter described

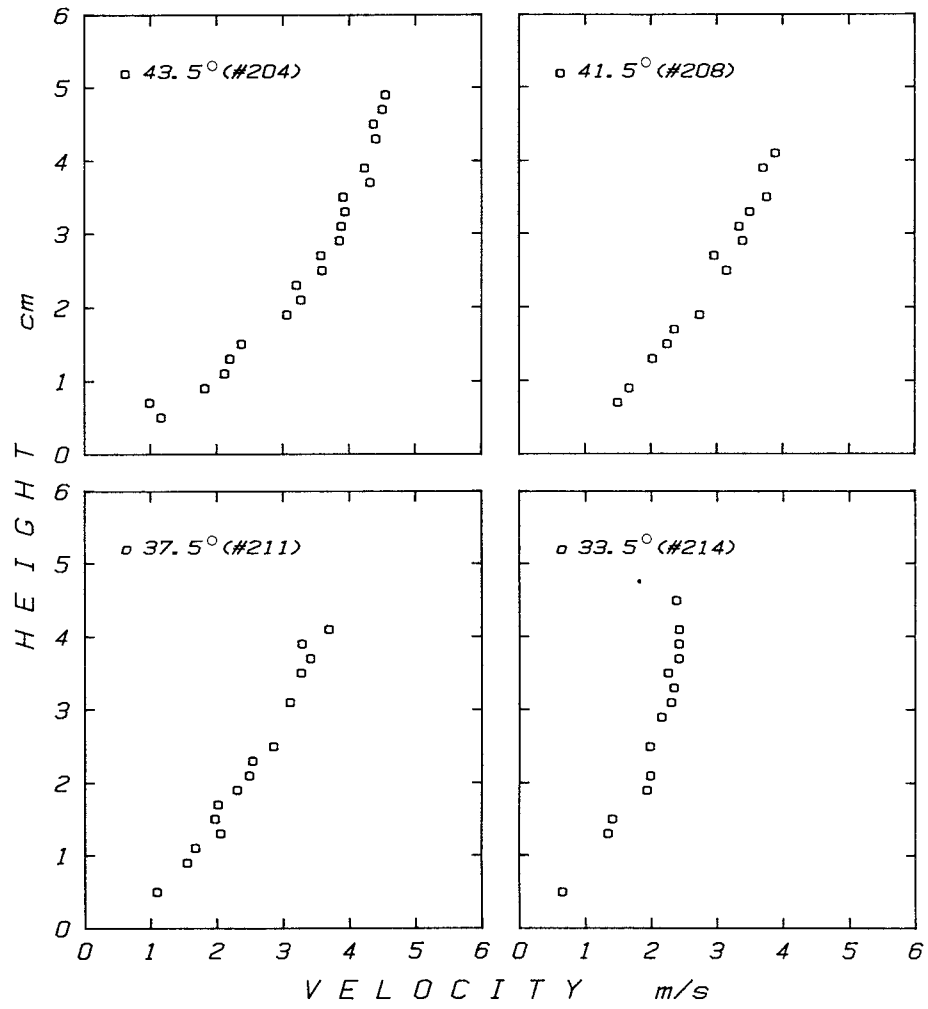

Fig. 14 Velocity profiles at various chute-inclinations.

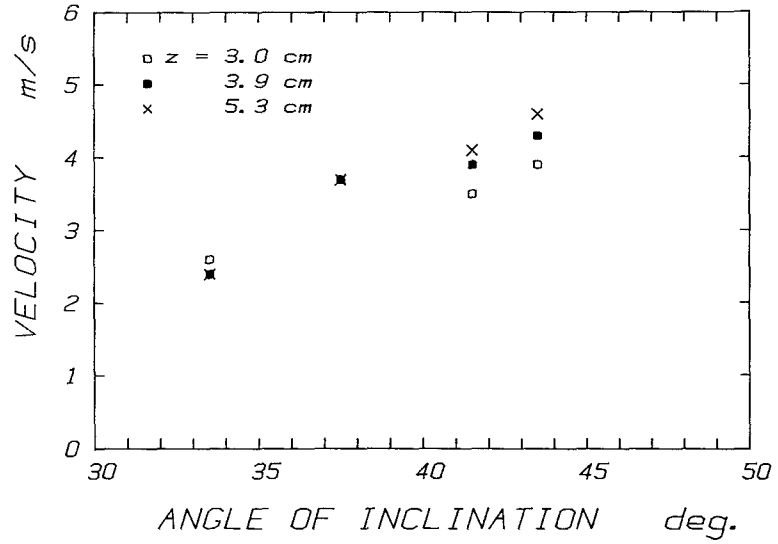

Fig. 15 Snow flow velocities versus chute angles.

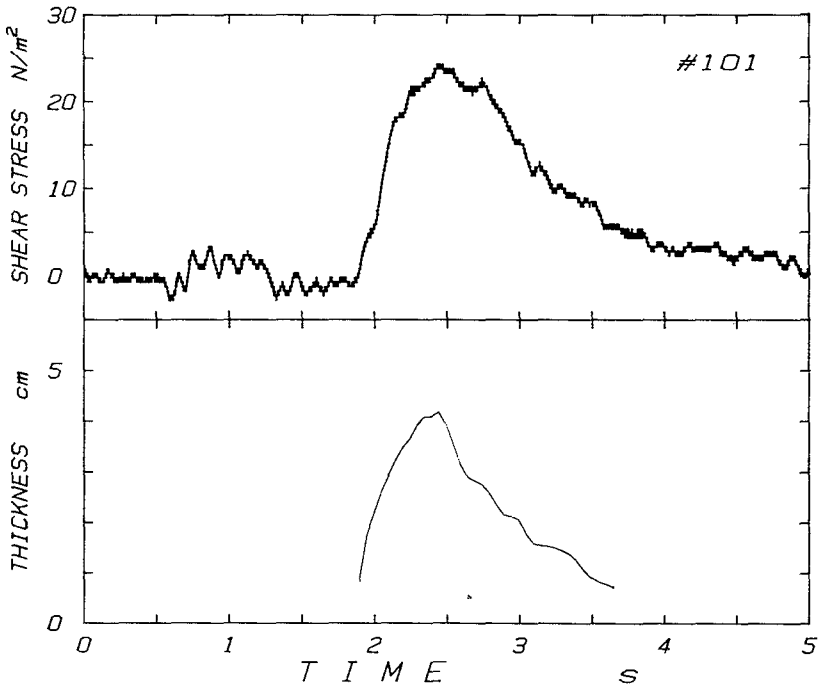

Fig. 16 Time variation of basal shear stress and snow flow thickness.

previously. Fig.16 shows a typical example of recordings of basal shear stress and snow flow thickness. There were much noises in the shear force signals, which were eliminated with a low-pass filter having a cut-off frequency of 17.5 Hz. The basal shear stress increases rapidly from the initial arrival of a snow flow and attains a fairly constant value for 1 s before its decrease. It is shown that in the steady state part of the snow flow, where the thickness and velocities are roughly constant as shown in Figs. 11 and 12, the shear stress also remains constant.

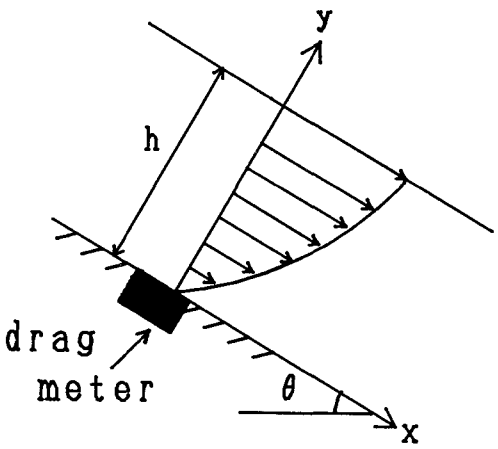

Fig. 17 Two-dimensional snow flow down an inclined chute.

For a steady, two-dimensional, fully developed, free surface granular flow down a rough plane inclined at angle θ as shown in Fig. 17, normal and shear stresses on a plane parallel to the bed are given by the following momentum equations

$$\tau_{yy}=g\cos\theta\int_y^h \rho dy \qquad (2)$$

and $$\tau_{xy}=g\sin\theta\int_y^h \rho dy \qquad (3)$$

where ρ is the bulk density and h is the thickness of snow flow. Since the average density throughout the depth $\bar{\rho}$ is expressed as

$$\bar{\rho}=\frac{1}{h}\int_y^h \rho dy \qquad (4)$$

the shear stress acting on the bed τ_b can be written as the following equation:

$$\tau_b=\bar{\rho}gh\sin\theta\ . \qquad (5)$$

Substituting into the Eq. (5) the value of τ_b and h measured directly with the drag meter and the high-speed video system respectively the average bulk density of snow flow $\bar{\rho}$ can be estimated. Densities of steady-state parts of snow flows, obtained were 100 to 200 kg/m^3, which were roughly comparable with the average density of overall snow flow estimated from depth, flow velocity and total weight of flowing.

c) Estimate of apparent viscosity coefficient of fluidized snow flow

The analyses described in the sections a) and b) gave the velocity profiles and densities of various fluidized snow flows. In this section we regard a snow flow as a continuum body and try to obtain a physical picture of a fluidized snow by comparing the observed data with

a theoretical model. As described in Fig. 17, for the steady, two dimensional, fully developed, free surface snow flow down a chute inclined at angle θ, the shear stress on a plane parallel to the bed is given by Eq. (3). Next we make two assumptions to get a preliminary picture of the snow flow property; First, the density is assumed to be uniform with depth. Eq. (5) then becomes

$$\tau_{xy}=\rho g(h-y)\sin\theta. \tag{6}$$

Second, we assume that the constitutive equation of the fluidized snow flow can be expressed

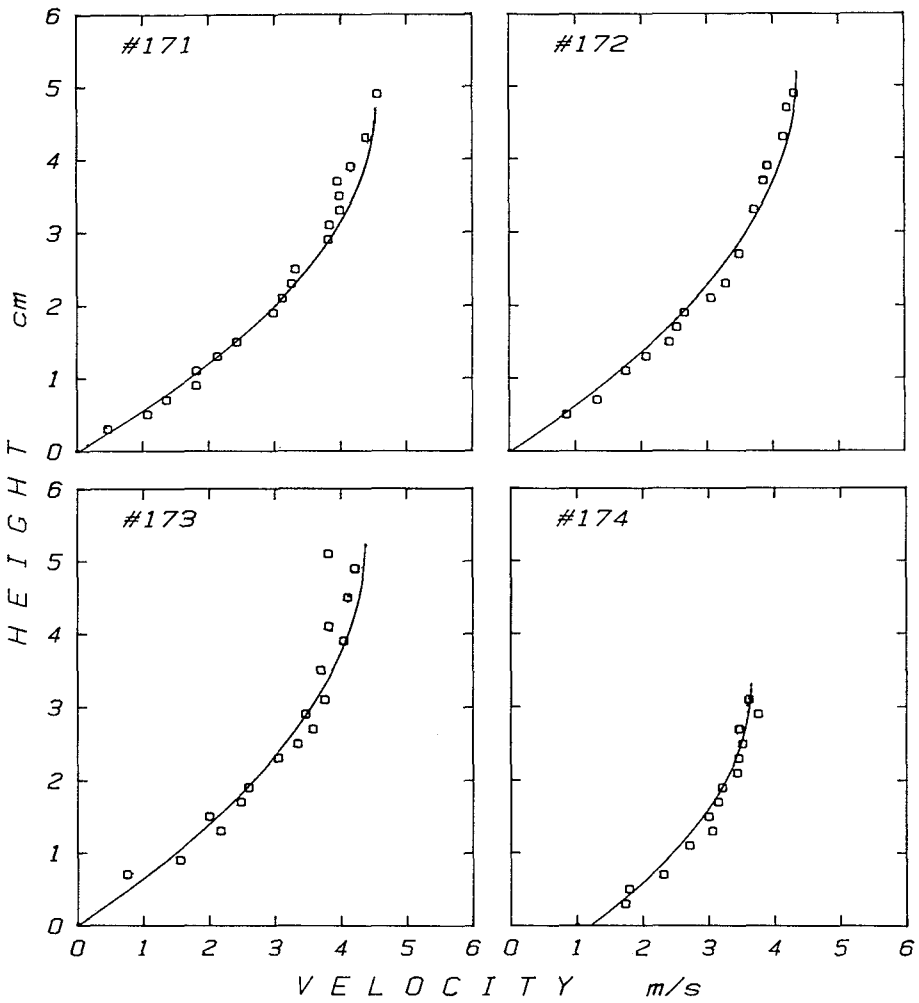

Fig. 18 Measured and calculated velocity profiles of snow flow (1). τ_0 is 0 N/m^2 for all cases.

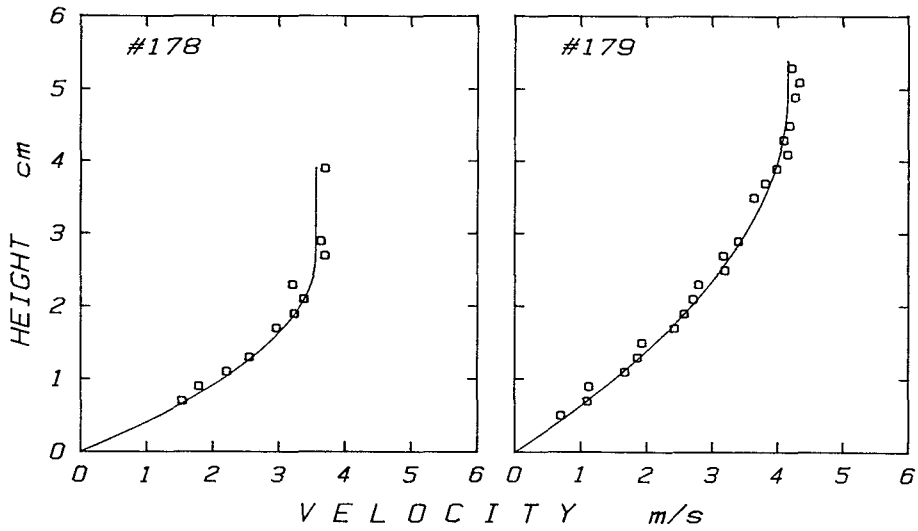

Fig. 19 Measured and calculated velocity profiles of snow flow (2). τ_0 is 10.5 N/m² and 3.5 N/m² for #178 and #179 respectively.

by

$$\tau_{xy}=\eta\frac{du}{dy}+\tau_0\ , \tag{7}$$

where η and τ_0 are constants depending on the flow property. According to the continuum theory this equation corresponds to the constitutive equation of a Bingham body, and in the special case of $\tau_0=0$ to a Newtonian body. Thus η represents the viscosity coefficient of fluidized snow; η estimated here will be named the apparent viscosity coefficient, however, since it is derived on the uncertain assumption of Eq. (7). From Eqs. (6) and (7) we see that

$$\frac{du}{dy}=\frac{(\rho g\sin\theta(h-y)-\tau_0)}{\eta}\ . \tag{8}$$

Integrating Eq. (8) from 0 to y, we obtain

$$u=\frac{\rho g\sin\theta}{\eta}\left(hy-\frac{y^2}{2}\right)-\frac{\tau_0}{\eta}y\ . \tag{9}$$

By using experimental values of ρ, θ, and h and comparing with observed velocity profiles, calculations were repeated to obtain best-fit values of η and τ_0 which make both R.S. and S.E. minima. Here R.S. is a square of residuals and S.E. is the standard error of the estimate. Figs. 18 and 19 show the calculated curves and experimental data in the case of $\tau_0=0$, whereas Fig. 20 shows the examples in which τ_0 have some finite values. Ten cases shown in Figs. 18, 19 and 20 are tabulated in Table 1. What is evident from the table is the apparent viscosity coefficients range from 8.3×10^{-2} to 4.5×10^{-1} Ns/m² and τ_0 is 0 to 10 N/m² for the densities of 100 to 200 kg/m³. The apparent viscosity coefficients are plotted versus bulk

snow densities for all the examples in Fig. 21. Although dispersion of data is rather large it is seen that the viscosity increases with density in this density range from 120 to 200 kg/m^3. Bucher & Roch (1946), Lang & Dent (1982) and Casassa et al. (1989) obtained viscosity coefficients of fluidized snow with their block-sliding experiments as mentioned before. Their data are tabulated in Table 2. Their values roughly agree with those obtained in this chute experiment. In particular values of Casassa (1989) in a similar density range give fairly good agreement.

Suzuki & Tanaka (1971) performed chute experiments with glass beads, calcite and sand

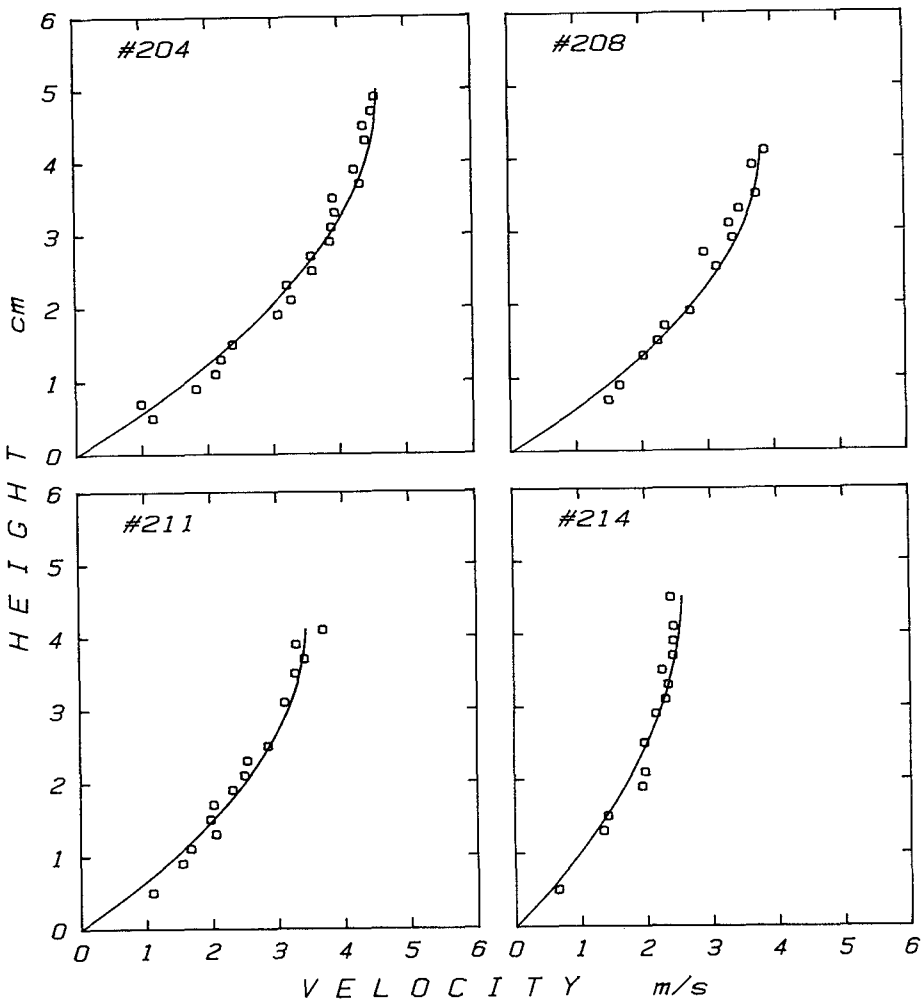

Fig. 20 Measured and calculated velocity profiles of snow flow (3). τ_0 is 0 N/m^2 for all cases.

Table 1 Data of the snow flow velocity profiles and results of numerical calculations with Eq. (19)

Run	θ (deg)	u_s (m/s)	h (cm)	ρ (kg/m^3)	η (Ns/m^2)	τ_0 (N/m^2)	R.S.	S.E.
171	43.5	4.4	4.8	140	2.4×10^{-1}	0	0.88	0.22
172	43.5	4.3	5.2	110	2.3×10^{-1}	0	1.20	9.27
173	43.5	4.1	5.3	120	2.6×10^{-1}	0	0.71	0.20
174	43.5	3.6	3.3	120	1.8×10^{-1}	0	0.46	0.18
178	43.5	3.7	4.0	120	8.3×10^{-1}	10.5	0.22	0.14
179	43.5	4.3	5.4	120	2.4×10^{-1}	3.5	0.48	0.15
204	43.5	4.5	5.0	190	3.5×10^{-1}	0	0.23	0.10
208	41.5	3.8	4.2	200	3.0×10^{-1}	0	0.19	0.12
211	37.5	3.7	4.2	150	2.3×10^{-1}	0	4.0×10^{-3}	1.7×10^{-2}
214	33.5	2.4	4.6	200	4.5×10^{-1}	0	1.2×10^{-4}	3.0×10^{-3}

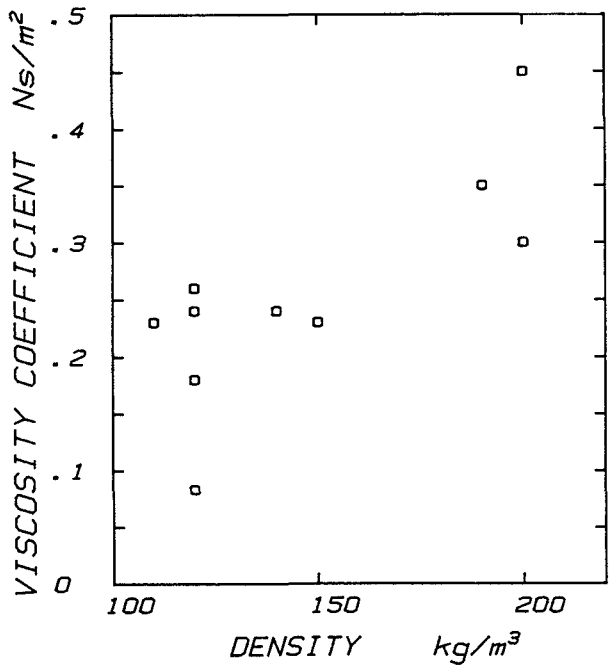

Fig. 21 Apparent viscosity coefficients of fluidized snow flow versus bulk snow densities.

Table 2 Viscosity coefficients of the fluidized snow obtained by other researchers

	η (Ns/m²)	ρ (kg/m³)
Bucher & Roch (1946)	0.9	300
Lang & Dent (1982)	0.2~1.0	400
Casassa et al. (1989)	6.6×10^{-2}~4.8×10^{-1}	150

Table 3 Viscosity and yield stress of granular materials. (Suzuki and Tanaka, 1971)

	η (Ns/m²)	τ_0 (N/m²)
Glass beads	2.5×10^{-1}	27
Calcite	8.0×10^{-2}	57
Sand	1.5×10^{-1}	47

flowing down a 1.2 m long chute. They obtained the shear stress and the shear stress of the flow indirectly from the flow rate, flow thickness, and chute angle, etc.; they analyzed their data with a Bingham body model; Obtained viscosity coefficients and yield stress (τ_0) are shown in Table 3. Comparing the data in Tables 1 to 3 we can conclude that viscosity coefficient of various particle flows are roughly similar although physical properties of individual particles are fairly different.

It should be noted that apparent viscosity coefficient obtained above depends on an assumption especially of the linear relation between τ and du/dy (Eq. (7)); The assumption will be shown to be adequate only at a smaller range of du/dy in Chapter V.

III.4. *Conclusions*

Inclined chute experiments of snow flows were carried out in a cold laboratory in order to investigate the mechanical properties of fluidized snow. According to the measurements: In the steady state part of the snow flow, where the thickness and velocities are roughly constant, the snow flow generally consists of two layers, snow-dust and flowing layers, and the velocity profiles in the flowing layer obtained were discussed with a flow model. Densities of the steady-state part of snow flow, obtained by substituting τ_b measured directly with the drag meter into Eq. (5), were 100 to 200 kg/m³. By assuming the density is uniform with depth and the constitutive equation of the fluidized snow flow can be expressed by Eq. (7), the apparent viscosity coefficients η was estimated to range from 8.3×10^{-2} to 4.5×10^{-1} Ns/m² and yield stress τ_0 from 0 to 10 N/m².

IV. Fluidized-bed experiments of snow

In order to investigate in greater detail the dynamical property of fluidized snow, in particular its dependence on bulk density, particle size and shape, a series of viscosity experiments were carried out with a fluidized-bed of snow.

IV.1. *Apparatus and procedures*

Fig. 22 shows the experimental apparatus used for generating the fluidized snow. Snow in a fluidized state was produced by the imposition of a vertical, upward air flow from the bottom of the snow contained in a transparent tube of 75 mm internal diameter. The flow rate could be regulated and measured with a flow meter in a range from 1.3×10^{-3} to 4.2×10^{-3} m^3/s.

The surface of the fluidized snow was observed from the side of the apparatus using the high-speed video system. It seems to be reasonable to assume that the bulk snow density does not change with depth in the fluidized snow, as the viscosity measured by Maeno and Nishimura (1978) is fairly constant all-over the depth. Thus we calculated the bulk density of fluidized snow from the mass and volume of snow in the tube. The measurements were made at temperatures of -12.3°C and -32.7 °C.

The viscous property of the fluidized snow was studied with a Brookfield viscometer (Tokyo Keiki, BM-type) and a modified Stormer-type viscometer (Ueshima, VR-901). The fundamental part of the former is shown schematically in Fig. 23. The instrument is powered by a synchronous induction-type motor to ensure that the speed of rotation will be constant. Torque power (N) is transmitted to a cylindrical rotor of 19 mm in diameter and 64 mm high through a transmission and a spring which is pre-calibrated. When the rotor is immersed in a sample fluid, a viscous drag opposes the rotation of the motor. This drag is detected as a strain on a spring register as deflection (θ). If the sample is a Newtonian fluid,

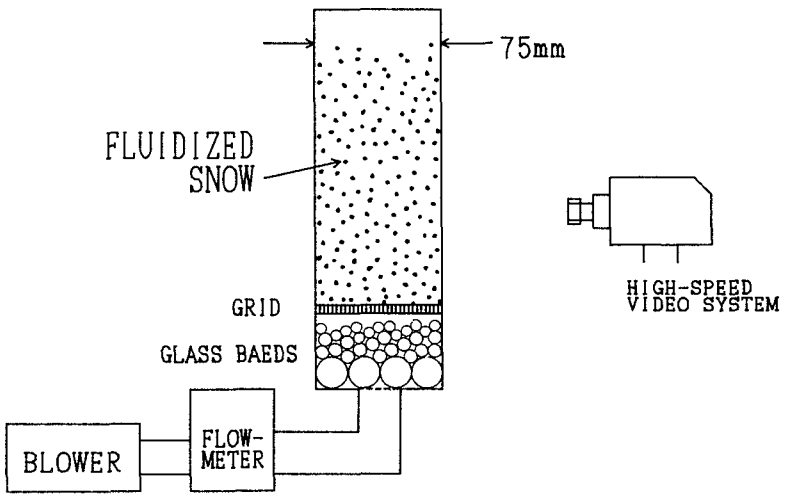

Fig. 22 Schematic diagram of the experimental apparatus for generating the fluidized snow.

its viscosity coefficient can be read directly on the indicator. What is more important, the shear stress τ and the shear rate du/dy can be estimated independently as functions of θ and N respectively,

$$\tau = K_1 \theta \tag{10}$$

and

$$\frac{du}{dy} = K_2 N \tag{11}$$

where K_1 and K_2 are constants to be determined in a standard oil (JS100−20H). Thus the relation between the shear stress and the shear rate, that is a flow curve, can be obtained, even if the sample is a non-Newtonian fluid.

Since the Brookfield viscometer is not sensitive to the viscosities less than 1×10^{-3} Ns/m^2, a modified Stormer-type viscometer was also used as a supplementary method. As shown in Fig. 24, the rotor consists of two paddles with dimensions 18 mm×7 mm×0.5 mm or 28 mm×7 mm×0.5 mm. A constant torque was applied to the rotor set in the fluidized snow and the time for 100 revolutions, t_{100}, was measured. The t_{100} value was converted to the absolute viscosity coefficient by calibration with standard oil. The calibration curves which show the relation between t_{100} and the viscosity coefficient are shown in Fig. 25. Owing to the complicated rotor configurations, this viscometer can not specify correct values of shear stress and shear rate.

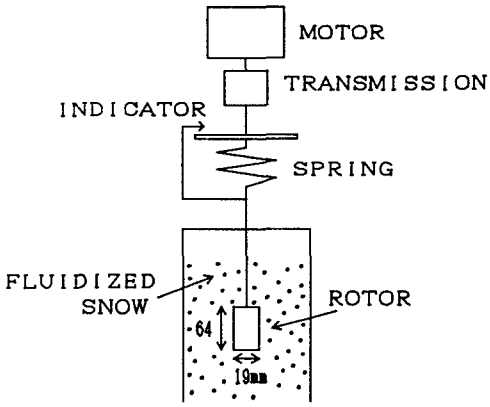

Fig. 23 Brookfield viscometer.

Viscosity coefficients were also measured with both the viscometers in the same

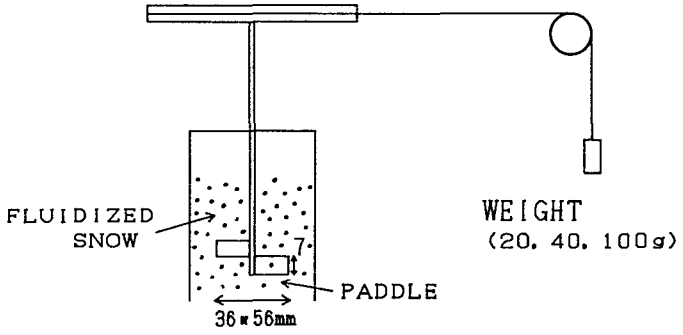

Fig. 24 Modified Stormer-type viscometer.

tube without snow in various upward air flow conditions, giving constant values, from which we can assume that the vertical air flow itself does not influence the viscosity of the fluidized snow.

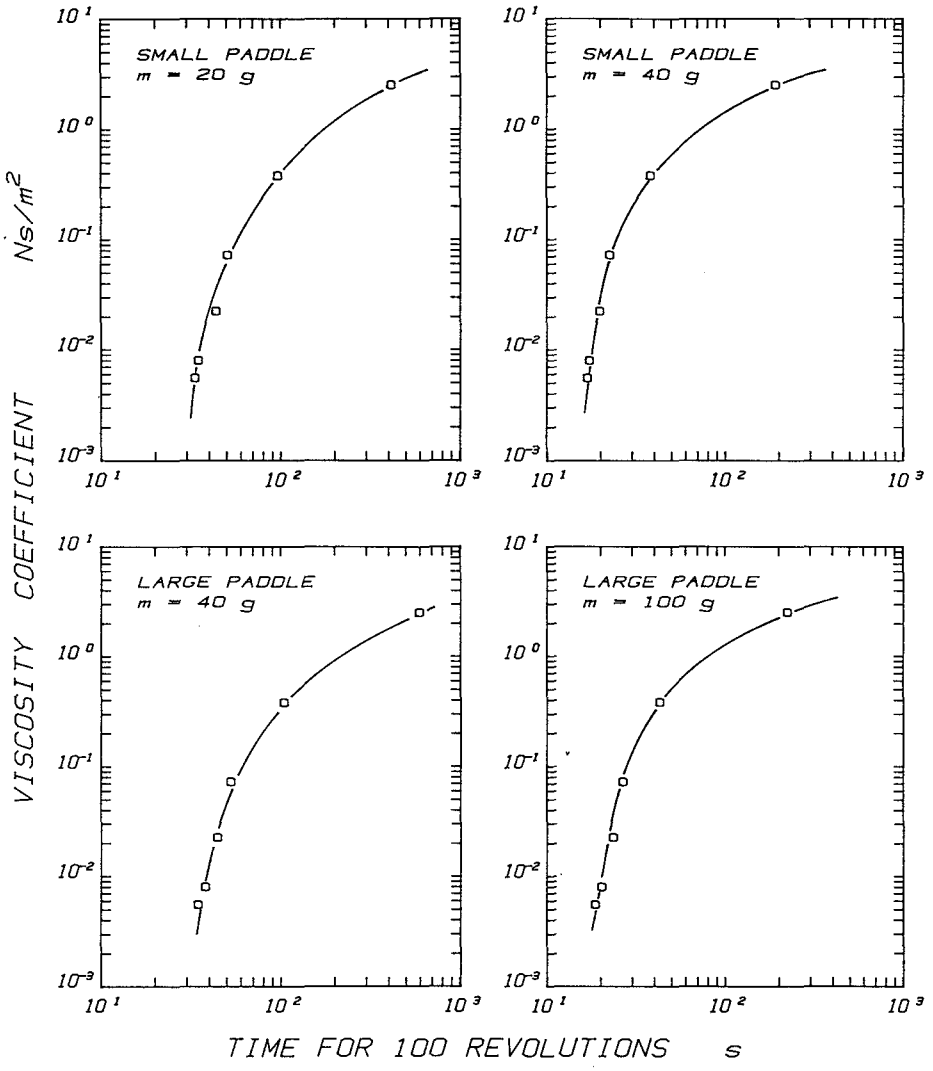

Fig. 25 Viscosity coefficients versus t_{100} measured with the modified Stormer-type viscometer.

IV.2. *Snow samples*

Experiments were performed with the following four kinds of snow samples, designated as sample A, B, C and D. Fig. 26 gives histograms of particle sizes of the samples. Particle sizes are expressed as diameters of circles with equivalent projected areas, which were measured from enlarged microphotographs containing 300−500 particles. Statistical prop-

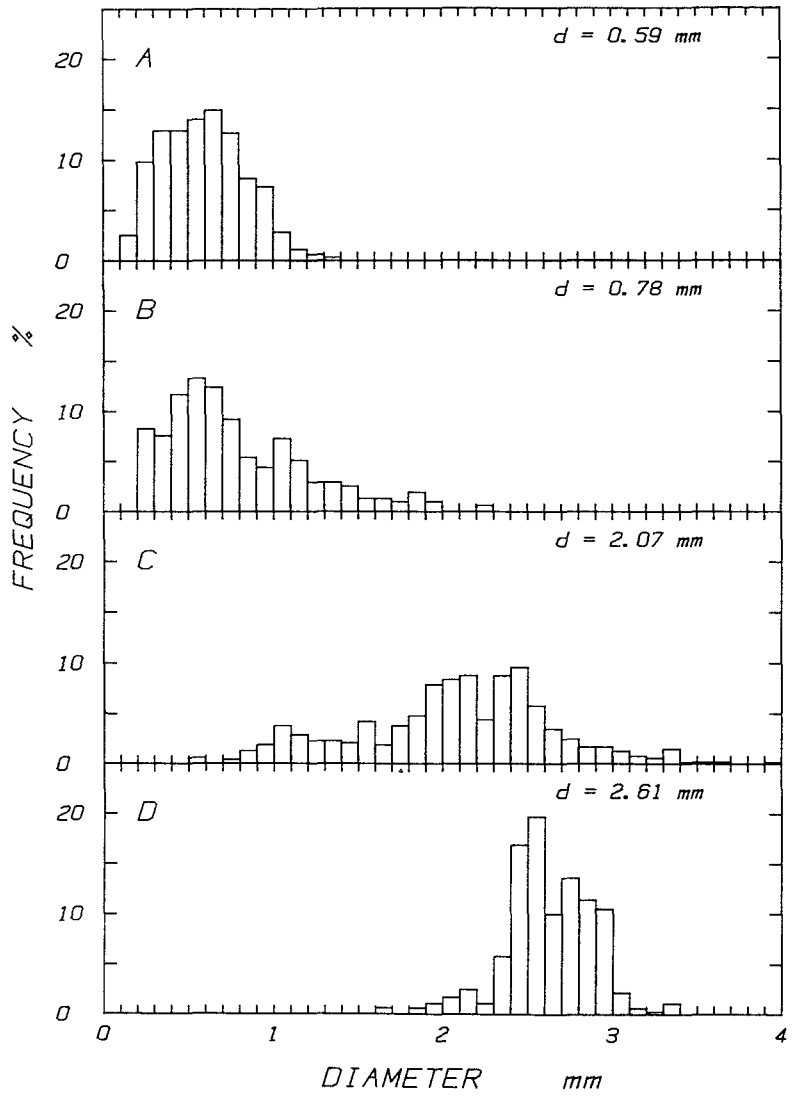

Fig. 26 Histograms of snow particle diameters.

Table 4 Properties of snow samples

Sample	Number of cases	Mean (mm)	Standard deviation (mm)	Coeff.of variation	Skewness	Kurtosis	Mean deviation (mm)	Median (mm)
A	355	0.95	0.24	0.41	0.32	-0.41	0.20	0.57
B	314	0.78	0.42	0.54	1.03	0.69	0.34	0.67
C	478	2.06	0.58	0.28	-0.20	-0.04	0.46	2.11
D	360	2.60	0.33	0.13	-2.94	21.0	0.22	2.60

erties of each sample are listed in Table 4.

A and B are natural fine-grained snow, which were collected from the suburbs of Sapporo city. A was kept in a cold room at −10 °C for about eight months and B almost twenty months before use. B is about 0.2 mm larger than A in regard to the mean diameter d. Sample C of average diameter 2.06 mm was obtained with sieving the granular snow kept in a cold room over two years. Sample D is ice spheres which were made by dropping pure water droplets from an injector and freezing in liquid nitrogen. The spheres were sieved to give a uniform average diameter of 2.60 mm with a standard deviation of 0.33 mm. As is shown in Table 4, the particle size of D is almost uniform; the coefficient of variation, which is the amount of the standard deviation divided by the mean value, is quite small and the kurtosis is very large. The skewness and the kurtosis of A and C are small enough to assume that the size distributions can be regarded as normal ones. It is sample A that was used in the chute experiment described in Chapter III. Considering that the skewness of B is rather large and the median diameter of B is different from the mean (arithmetic mean particle diameter d), B is somewhat deviated from a normal distribution. Further, with reference to Fig. 26, we might consider that sample B is the mixture of rather big particles with sample A. Fig. 27 shows the contour ratio r given as

$$r=\frac{\text{Perimeters of projected areas}}{\text{Perimeters of circles with equivalent projected areas}}. \tag{12}$$

Since r of D is almost unity, sample D can be approximated as spheres. On the other hand r of other samples shows a similar distribution, being over 1.5.

IV.3. *Results*

Figs. 28 (A−D) show the shear stress versus the shear rate obtained in the fluidized-bed of snow with the Brookfield viscometer. Results are presented for four different densities. Each set of data in Fig. 28, plotted on a log-log coordinate, seems to be approximated with a straight line having a slope of unity. Thus the following expression is derived:

$$\tau=\eta\frac{du}{dy}+\tau_0. \tag{13}$$

The first term of the right side is a rate-dependent part, so η represents the viscosity coefficient of fluidized snow. The second term τ_0 is a rate-independent part. Since Eq. (13)

is identical to the constitutive equation of Bingham-body, τ_0 can be considered to be the yield stress of the fluidized-snow. Viscosity coefficients and τ_0 were calculated by applying a least-square fit to each set of data at a particular density. The results are listed in Table 5. Coefficients of correlation (r) were high enough in all the cases, thus we can conclude that fluidized snow behaves as a Bingham body in the range of density and shear rate measured. Viscosity coefficients of fluidized snow obtained ranged from 10^{-2} to 10^{-1} Ns/m^2; yield stress

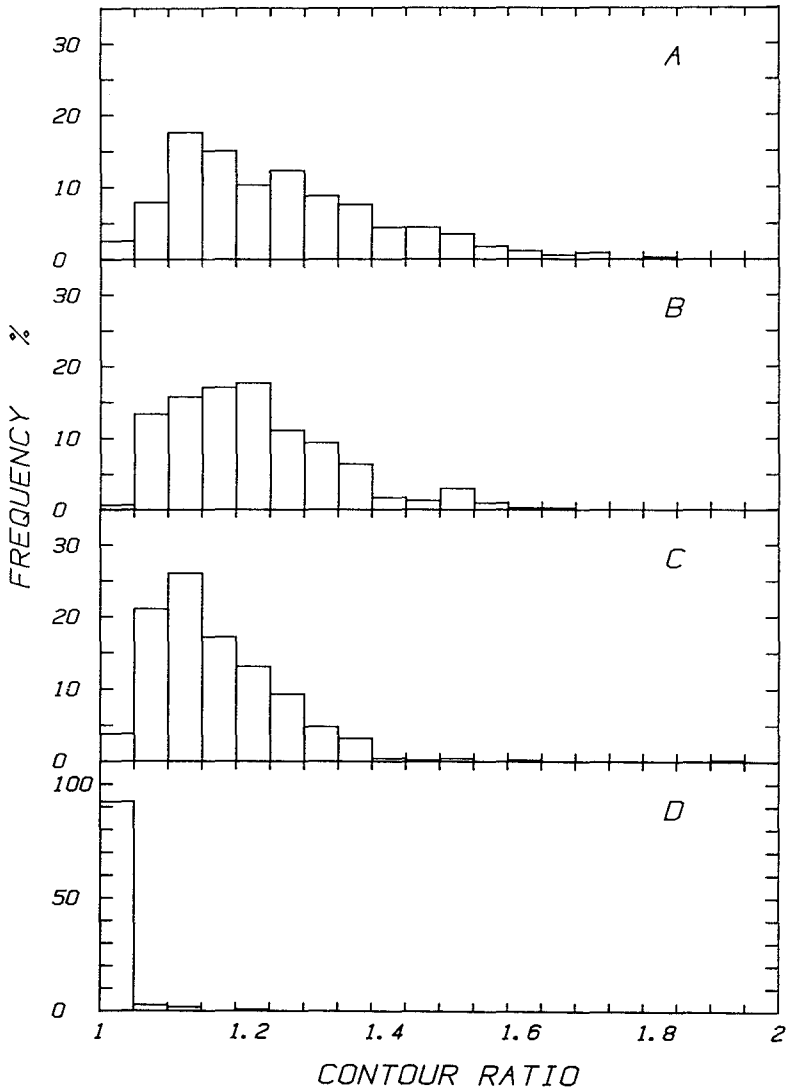

Fig. 27 Histograms of snow particle contour ratio r.

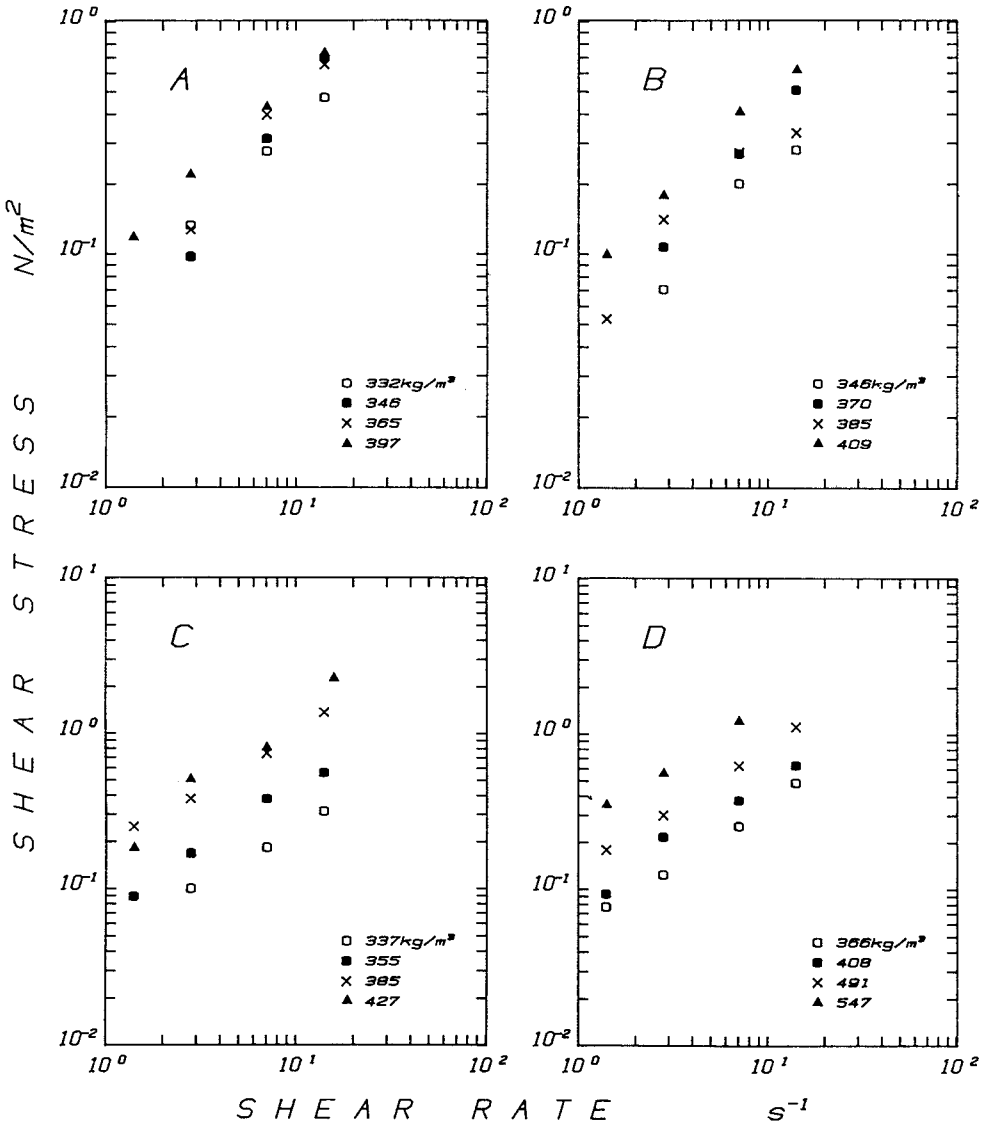

Fig. 28 Shear stress versus shear rate in the fluidized-bed of snow with the Brookfield viscometer.
A: $d=0.59$ mm, B: $d=0.78$ mm, C: $d=2.07$ mm and D: $d=2.61$ mm.

from 0 to 10^{-2} N/m^2; sometimes negative values of τ_0 appear due to the small magnitude and error involved in the experiment.

Table 5 Viscosity η and τ_0 obtained in the fluidized-bed of snow. r shows the correlation coefficient.

	ρ kg/m^3	η Ns/m^2	τ_o N/m^2	r
A (d=0.59mm)	332	3.0×10^{-2}	5.6×10^{-2}	> 0.99
	346	5.5×10^{-2}	-6.0×10^{-2}	> 0.99
	365	4.7×10^{-2}	2.8×10^{-2}	0.99
	395	4.8×10^{-2}	7.4×10^{-2}	> 0.99
B (d=0.79mm)	346	1.8×10^{-2}	4.1×10^{-2}	0.96
	370	3.6×10^{-2}	1.3×10^{-2}	> 0.99
	385	2.1×10^{-2}	6.9×10^{-2}	0.93
	409	4.1×10^{-2}	6.8×10^{-2}	0.99
C (d=2.07mm)	337	2.0×10^{-2}	4.8×10^{-2}	> 0.99
	355	2.0×10^{-2}	4.8×10^{-2}	0.98
	385	9.1×10^{-2}	1.3×10^{-1}	> 0.99
	409	1.4×10^{-1}	-2.6×10^{-2}	0.99
D (d=2.61mm)	366	3.3×10^{-2}	3.1×10^{-2}	> 0.99
	408	4.2×10^{-2}	7.2×10^{-2}	> 0.99
	491	7.5×10^{-2}	9.0×10^{-2}	> 0.99
	547	1.5×10^{-1}	1.3×10^{-1}	> 0.99

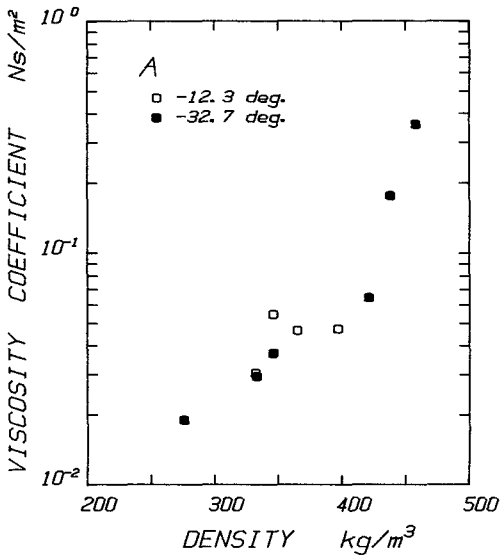

Fig. 29 Viscosity coefficients versus bulk densities for sample A (d=0.59 mm).

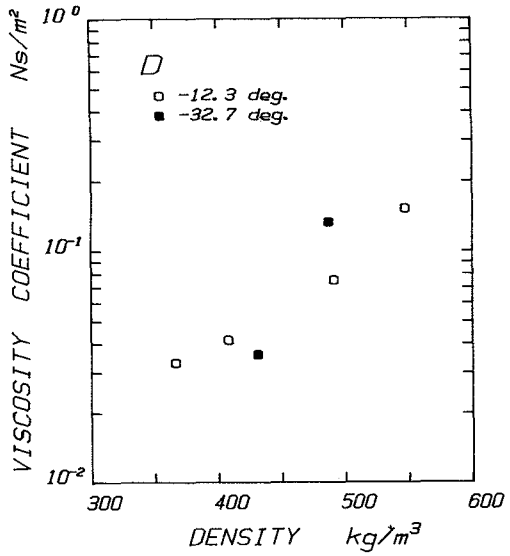

Fig. 30 Viscosity coefficients versus bulk densities for sample D (d=2.61 mm).

The dependences of the viscosity coefficient upon the bulk density are shown in Fig. 29 for sample A, in Fig. 30 for D and in Fig. 31 for all the samples. In Figs. 29 and 30, viscosity coefficients obtained at −37.3 ℃ as well as −12.3 ℃ are plotted. The effect of temperature on the viscosity coefficient of fluidized snow does not seem important in this temperature range, but the effect might become important at much higher temperatures near the melting point of ice because of the increasing adhesion between snow particles. A strong increase in viscosity with density can be observed for all snow samples. An exponential function of the following form provides a good fit:

$$\eta = a \exp(b\rho) \tag{14}$$

where a and b are constants. Results for all samples are summarized in Table 6.

Maeno et al. (1980) obtained a strong dependency of viscosity with particle diameter: viscosity coefficient is larger for snow with larger particles. But the effect of particle diameter is not clear in Fig. 31 since four samples (A, B, C and D) used here are not only

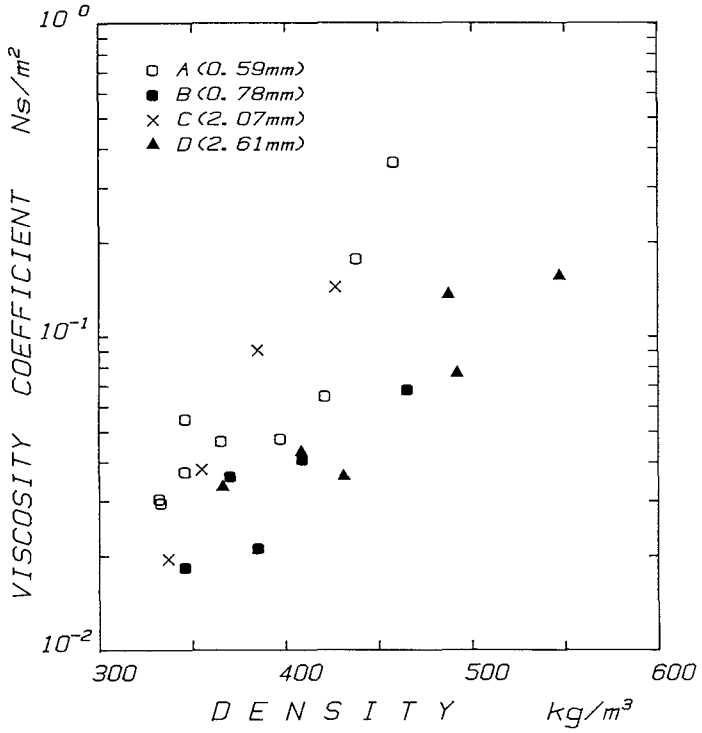

Fig. 31 Viscosity coefficients versus bulk densities for all samples.: sample A (d=0.59 mm), B (d=0.78 mm), C (d=2.07 mm) and D (d=2.61 mm).

Table 6 Viscosity of the fluidized-bed of snow as a function of bulk density. a and b represent the parameters of equation : $\eta = a \exp(b\rho)$; shows the correlation coefficient.

	a	b	r
A(d=0.59mm)	8.97×10^{-4}	9.42×10^{-3}	0.91
B(d=0.79mm)	1.46×10^{-5}	2.19×10^{-2}	0.97
C(d=2.61mm)	5.62×10^{-4}	1.03×10^{-2}	0.88
D(d=2.61mm)	2.88×10^{-4}	1.42×10^{-2}	0.91

different in the mean diameter but also in size distribution and contour ratio as shown in Fig. 26 and Fig. 27.

τ_0 seems to be a monotonic increasing function of the density. Fig. 32 shows the case of sample D. It is evident that τ_0 increased exponentially with density in the same manner as the viscosity. On the other hand, the shear strength of bonded snow is in a range 10^2 to 10^3 N/m^2 at the density of 100 to 200 kg/m^3 (Mellor, 1974). It seems to be reasonable to consider that the yield stress of fluidized snow is about two orders of magnitudes smaller than that of bonded snow.

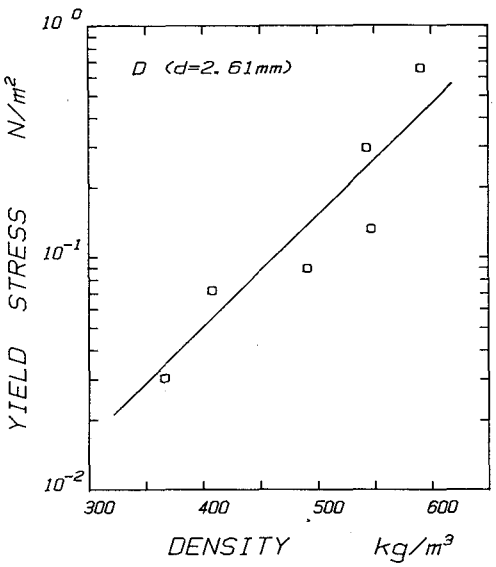

Fig. 32 Shear rate versus τ_0 in the fluidized-bed of snow (sample D).

As mentioned above, the sensitivity of Brookfield viscometer is not good for viscosity coefficients less than about 10^{-2} Ns/m^2, what is worse it cannot be used to measure values under 10^{-3} Ns/m^2. Figs. 33(A)−(D) show the viscosity coefficients of fluidized bed of snow obtained from the modified Stormer-type viscometer in addition to those from Brookfield viscometer. It is seen that both the viscometers give similar results, furthermore the data measured with the Stormer-type viscometer are on the extension of the data with the Brookfield viscometer. The values of the viscosity coefficient at a density of 200 kg/m^3 lie around 10^{-3} Ns/m^2(see Fig 33(a)), which is comparable to that of liquid water at ordinary room temperature.

IV.4. *Conclusions*

Fluidized snow was produced in a fluidized-bed experiment system, and its viscous properties were measured with a Stormer-type viscometer and Brookfield viscometer which gives the shear stress and the shear rate independently. All the sets of data obtained could

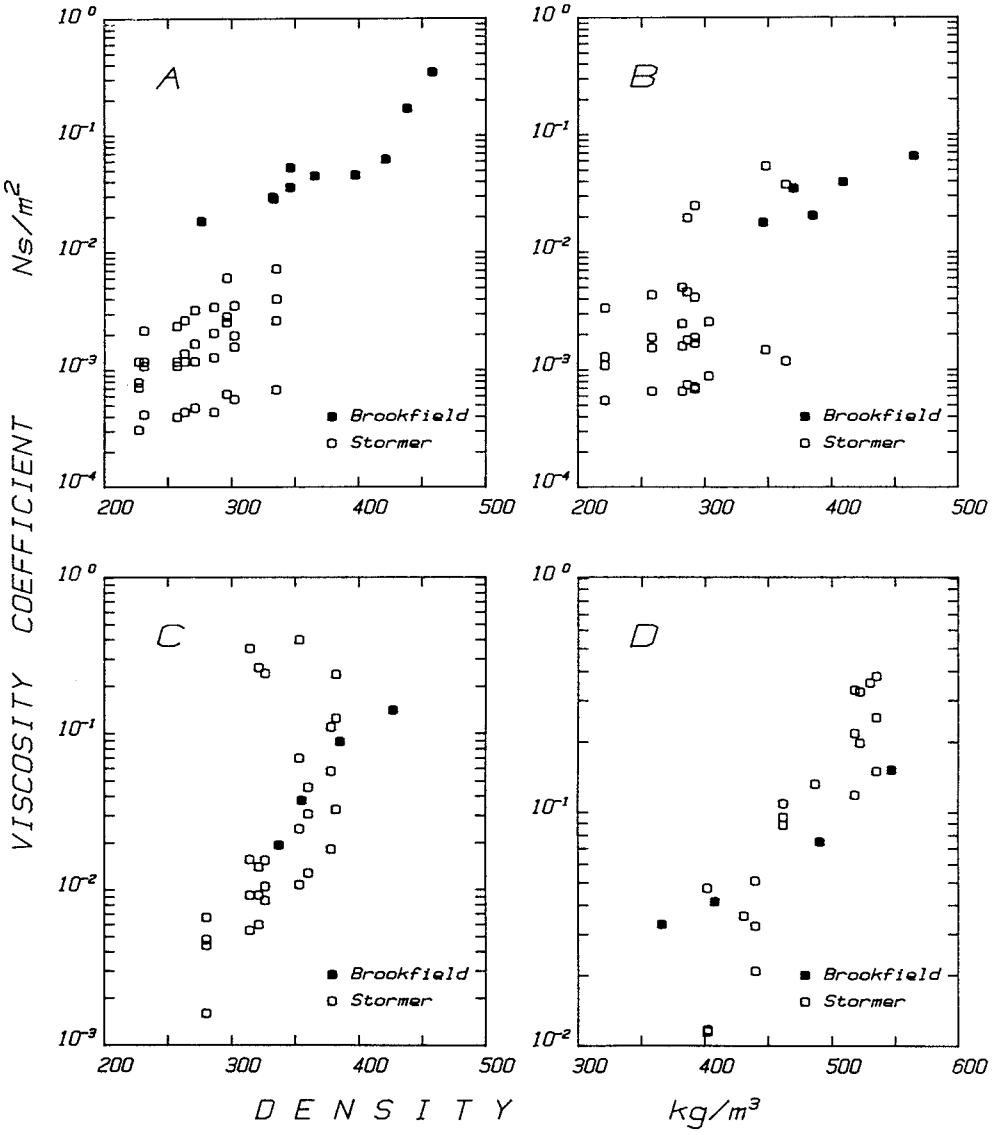

Fig. 33 Viscosity coefficients of the fluidized-bed of snow measured with the Brookfield viscometer and the modified Stormer-type viscometer.

be expressed with Eq. (13) reasonably; Thus we can conclude that the fluidized snow behaves as a Bingham body in the range of the density (250 to 450 kg/m^3) and the shear rate (1 to 15 s^{-1}) measured. Viscosity coefficients of fluidized snow obtained ranged from 10^{-2} to 10^{-1} Ns/m^2; yield stress from 0 to 10^{-2} N/m^2. A strong increase in the viscosity coefficient with the density was observed, which could be expressed with the exponential function of Eq. (14).

V. Dynamical properties of fluidized snow

Dynamical properties of the fluidized snow were studied with two types of experiments: one is the inclined-chute experiment discussed in Chapter III and the other is the fluidized -bed system experiment discussed in Chapter IV. In this chapter first we compare the viscosity coefficients obtained in the two different systems in special reference to the shear rate of each experiment. Then we reanalyze the velocity profiles found in the chute flows. And finally a constitutive equation which describes the general dynamical properties of fluidized snow is proposed.

V.1. *Comparison of the viscosities obtained by the chute and fluidized-bed experiments*

The apparent viscosity coefficients of fluidized snow obtained in the chute experiment were 1×10^{-1} to 5×10^{-1} Ns/m^2 at the density of 200 kg/m^3 as shown in Table 1. On the other hand, viscosity coefficients obtained in the fluidized-bed system were 10^{-3} to 10^{-2} Ns/m^2 at the same density range (Fig. 33). The former are about one to two orders magnitude larger than the latter. If the fluidized snow acts as a Bingham body following Eq. (7), the viscosity coefficient should be constant; Obviously the Bingham or Newtonian model cannot explain simultaneously the results obtained in the two systems. In discussing the conflict it should be noted that in the fluidized-bed experiment the shear stress and the shear rate were measured independently, giving a linear relation between them; On the other hand, a Bingham body model and uniform density profile were assumed in the chute experiment. Furthermore if we estimate the shear rate of the chute experiments it amounts to 60 to70 s^{-1}, which is roughly ten times larger than that in the fluidized-bed experiments (1 to 15 s^{-1}).

Fig. 34 shows the relation between the shear stress and shear rate for the chute experiment. The shear stress was measured with the drag meter, and the shear rate was calculated from the velocity difference between the surface and bed of snow flow and the flow thickness h. Due to insufficient data wide dispersion of the data is found (the density, 120 kg/m^3 and 150 kg/m^3). But for the density of 200 kg/m^3, the shear stress versus shear rate plotted on log-log paper has a slope of 2 rather than 1, i.e. the shear stress varies as the square of shear rate.

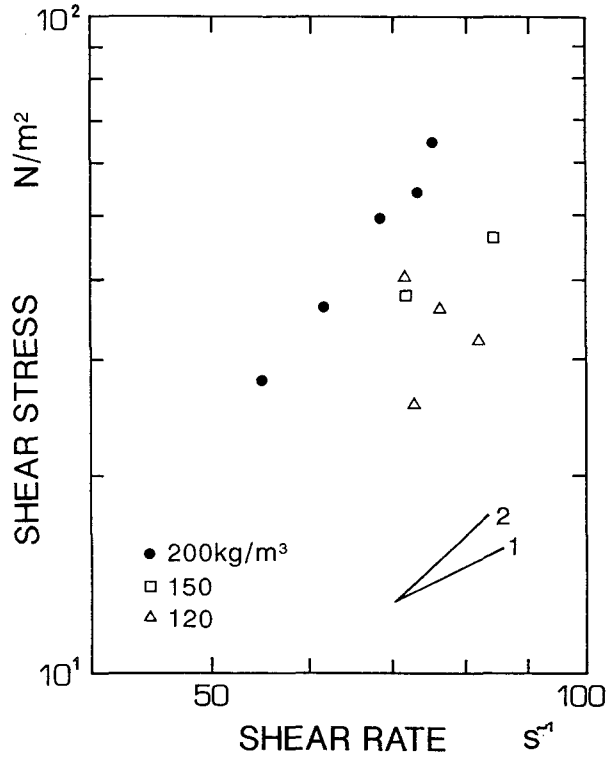

Fig. 34 Relation between the shear stress and the shear rate for the fluidized-snow obtained with the inclined chute experiments.

V.2. *Dynamical properties of fluidized snow under high shear rates*

With reference to the above discussion, we re-examine the assumptions made in the approximation of snow velocity profiles in Chapter III. Although we assumed ρ is uniform with depth in Eq. (6), it is considered to be more reasonable that the density of the lower part should be larger than that of the upper part. Then as a simplest model the bulk density of snow flow ρ is assumed to be a linear function of depth,

$$\rho = \rho_b - \frac{(\rho_b - \rho_s)\, y}{h} \tag{15}$$

where ρ_s and ρ_b represent the bulk density of the surface and bed respectively as shown in Fig. 35. ρ_s and ρ_b can be calculated in the following procedure: The average density over the depth ρ is written as

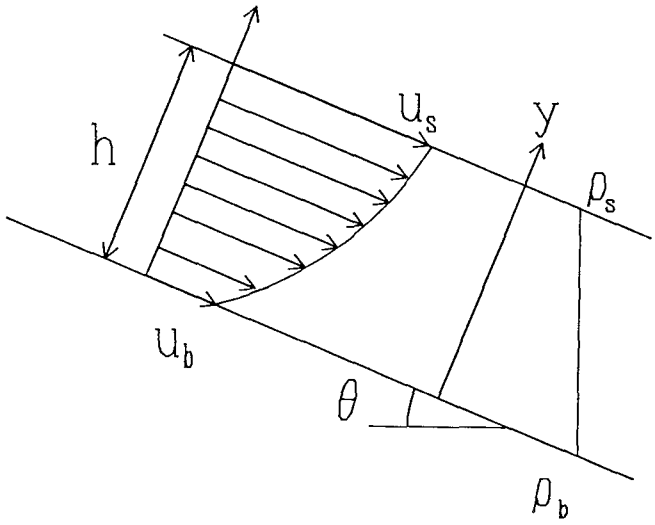

Fig. 35 Two dimensional snow flow down an inclined chute (II). ρ_s and ρ_b are bulk densities at surface and bed; u_b is a slip velocity.

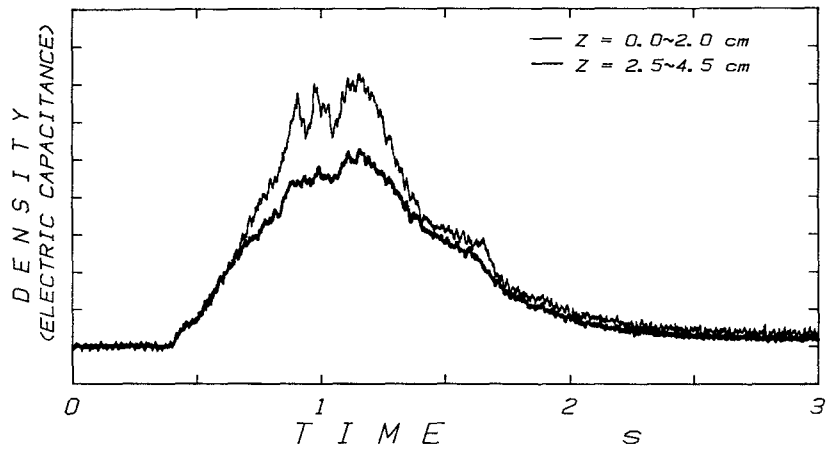

Fig. 36 Typical examples of the electric capacitance data. The unit of the vertical axis is arbitrary.

Table 7 Ratio of the bulk density at 10 mm to at 35 mm above the chute floor

Run	10	11	12	13	14	15	MEAN
C_2/C_1	0.77	0.71	0.71	0.78	0.74	0.72	0.74

$$\bar{\rho}=\frac{1}{h}\int_y^h \rho(y)\,dy=\frac{1}{h}\int_y^h \left(\rho_b-(\rho_b-\rho_s)\frac{y}{h}\right)dy$$
$$=\frac{(\rho_s+\rho_b)}{2}, \tag{16}$$

which can be calculated by substituting experimental values θ, h, and ρ_b into Eq. (5).

The electric capacitance ratio between 10 mm (C_1) and 35 mm (C_2) above the floor, which corresponds to the density ratio, was measured in some runs. This ratio was calculated with the data obtained in the steady-state part of the flow, where thickness and velocity are maintained almost constant. Typical examples of the capacitance data are shown in Fig. 36 and all the results are tabulated in Table 7. As is evident from the table, the density ratio is not so different in each flow and the mean of them is 0.74. Thus the following relation is derived from Eq. (15).

$$\rho_b-\frac{(\rho_b-\rho_s)}{h}\times 0.035=\left(\rho_b-\frac{(\rho_b-\rho_s)}{h}\times 0.010\right)\times 0.74 \tag{17}$$

Using Eq. (16) and Eq. (17), ρ_b and ρ_s can be calculated for individual snow flows.

Consequently the constitutive equation of fluidized snow is written as

$$\tau=\eta\frac{du}{dy}+\tau_0 \tag{18}$$

where η is not a constant but a product of shear rate and constant η_2 with reference to Fig. 34.

$$\eta=\eta_2\left(\frac{du}{dy}\right) \tag{19}$$

Thus Eq. (18) is rewritten as follows:

$$\tau=\eta_2\left(\frac{du}{dy}\right)^2+\tau_0 \tag{20}$$

Eq. (17) and Eq. (20) give

$$\frac{du}{dy}=\left(\frac{g\sin\theta\int_y^h \rho(y)\,dy-\tau_0(y)}{\eta_2(y)}\right)^{0.5} \tag{21}$$

When integrating Eq. (21) numerically, the following are assumed:

1) A slip velocity on the bed surface u_s was considered;

2) τ_0 obtained with the fluidized-bed system was as small as 10^{-2} N/m^2; τ_0 is ignored;

3) η_2 does not depend on y.

Substituting experimental values of ρ_b, ρ_s, θ and h, and comparing the obtained velocity profile, numerical integration with the Simpson formula was repeated to minimize both B.S.

and S.E. Fig. 37 shows typical examples of the calculated curves and experimental data. The results of nine cases are shown in Table 8. As is evident from these figures and table, both B.S. and S.E. are small; Thus we can conclude that the constitutive equation of fluidized snow (Eq. (20)) represents the actual velocity profile of snow flow; at high shear rates Eq. (20) can be applied for the fluidized snow.

η_2 is plotted versus bulk snow density for all the cases in Fig. 38. η_2 increases in this

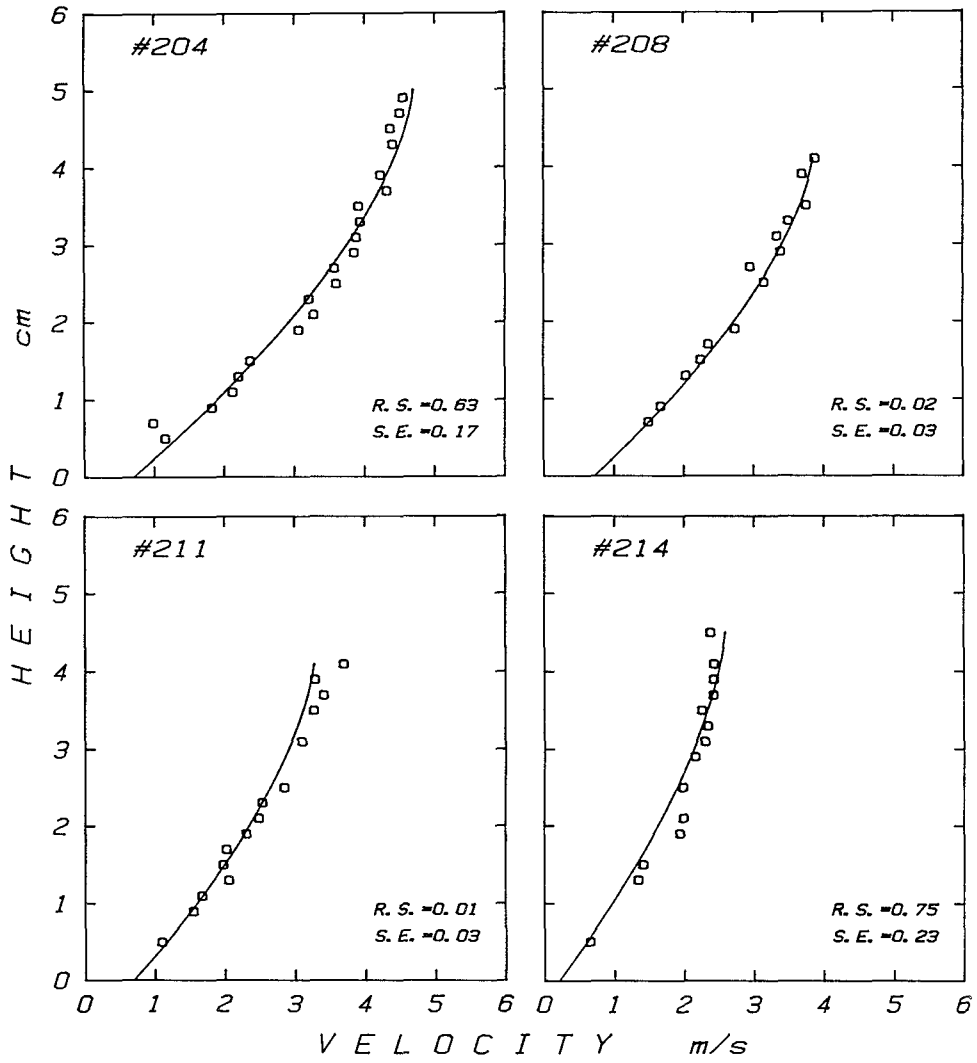

Fig. 37 Measured and calculated velocity profiles of snow flow (4). The solid curves represent the Eq. (21).

density range (100 to 200 kg/m^3), though the dispersion of data is rather large in a similar manner as apparent viscosity versus density in Fig. 21.

Table 8 Data of the obtained velocity profiles and results of numerical calculations with Eq. (21)

Run	θ (deg)	u_s (m/s)	h(cm)	$\bar{\rho}$ (kg/m^3)	ρ_b (kg/m^3)	ρ_s (kg/m^3)	u_b (m/s)	η_2	τ_o (N/m^2)	R.S.	S.E.
171	43.5	4.4	4.8	140	183	97	0.5	2.5×10^{-3}	0	3.6×10^{-1}	1.4×10^{-1}
172	43.5	4.3	5.2	110	146	74	0.3	2.0×10^{-3}	0	6.4×10^{-1}	2.0×10^{-1}
173	43.5	4.1	5.3	120	160	80	0.4	2.9×10^{-3}	0	2.5×10^{-1}	1.2×10^{-1}
174	43.5	3.6	3.3	120	142	98	1.2	2.0×10^{-3}	0	1.1×10^{-0}	2.8×10^{-1}
179	43.5	4.3	5.4	120	160	80	0.4	2.6×10^{-3}	0	2.2×10^{-1}	3.2×10^{-1}
204	43.5	4.5	5.0	190	249	131	0.7	3.9×10^{-3}	0	6.3×10^{-1}	1.7×10^{-1}
208	41.5	3.8	4.2	200	252	152	0.7	3.9×10^{-3}	0	1.5×10^{-1}	3.3×10^{-2}
211	37.5	3.7	4.2	150	189	114	0.7	4.0×10^{-3}	0	1.3×10^{-2}	2.9×10^{-2}
214	33.5	2.4	4.6	200	258	144	0.2	7.3×10^{-3}	0	7.5×10^{-1}	2.3×10^{-1}

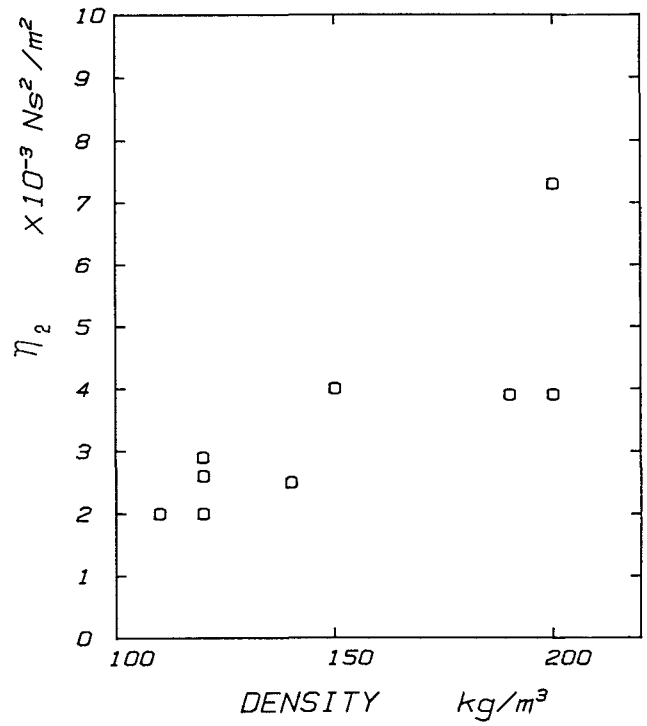

Fig. 38 η_2 of fluidized snow versus bulk density.

V.3. *Dynamical properties of fluidized snow*

Fig. 39 shows the shear stress versus the shear rate obtained from both the chute and the fluidized bed experiment. It is clear that shear stresses are linearly proportional to the shear rate in a lower shear rate region and shear stresses depend on the square of the shear rate in a higher shear rate region.

On the other hand in the field of soil mechanics and powder technology, annular shear cells have been developed to investigate the granular material behavior under rapid shear. The shear cell, for example, in Savage and Sayed (1984) consisted of two concentric disk assemblies mounted on a fixed shaft. Granular materials, such as sand or glass or polystyrene beads or crushed walnut shells, were contained in an annular trough in the bottom disk and capped by a lipped annular ring on the top disk. The bottom disk was rotated at specified rates while the top disk was loaded vertically and restrained from rotating by a torque arm connected to a force transducer. The apparatus was thus designed to determine the shear and normal stresses as functions of solids volume fraction and shear rate. Plots of these stresses as functions of the shear rate and particle concentration are found in published reports by Bagnold(1954), Savage and Mckeon(1983), Savage and Sayed(1984), Hunger and Morgenstern(1984) and Hanes and Inman(1985). Fig. 40 shows the shear stress

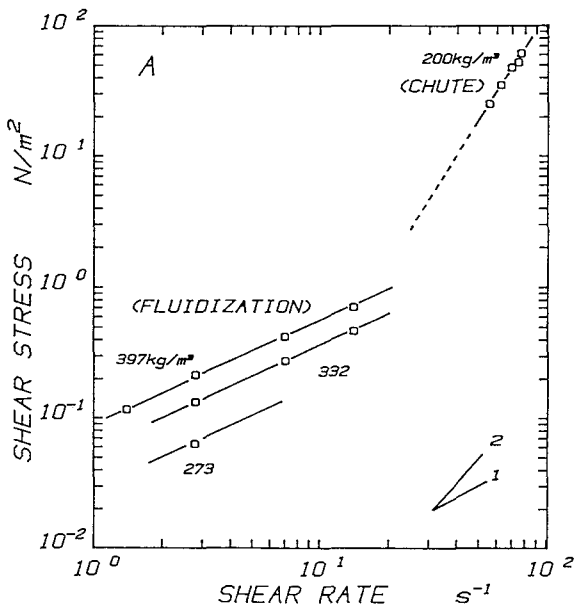

Fig. 39 Relation between the shear stress and the shear rate for the fluidized snow obtained with the inclined chute and the fluidized-bed experiments.

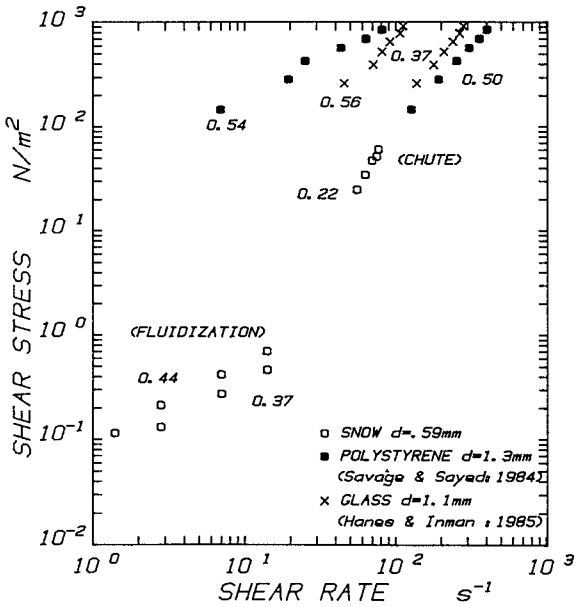

Fig. 40 Comparisons of the fluidized snow properties with polystyrene beads and glass beads ones.

versus the shear rate not only for snow obtained in this paper but also for polystyrene beads (Savage and Sayed, 1984) and glass beads (Hanes and Inman, 1985). Since the diameter and density of particles are different ($d=1.3$ mm and $\rho_s=1050$ kg/m^3 for polystyrene and $d=1.1$ mm and $\rho_s=2400$ kg/m^3 for glass), the absolute values of the measured shear stress varies, and the volume fraction of particles in the shear cell tests is larger than that of our snow experiment. But it is shown that the relations between shear stress and shear rate for glass and polystyrene are similar to those of fluidized snow: at higher shear rates over 10^2 s^{-1}, the shear stresses of glass and polystyrene were found to be proportional to the square of the shear rate, and at lower shear rates under 10^2 s^{-1}, be proportional to the shear rate raised to a power less than two.

A number of constitutive theories for granular flow have been proposed (Bagnold, 1954; Goodman and Cowin, 1971; Savage, 1979; Savage and Jeffrey, 1981; Jenkins and Savage, 1982): continuum theories or microstructural models have been formulated by considering collisional fluxes occurring during collisions. But a general theoretical solution has not been completed yet. Savage and Jeffrey (1981) have determined the stress tensor for a rapidly -sheared material by considering the exchange of momentum in collisions of smooth, perfectly elastic, spherical particles. The relative position and velocity of two particles are determined by plausible probability density functions. The normal and shear stresses are

determined as functions of a single nondimensional parameter R, which is the ratio of the characteristic mean shear velocity to the r.m.s. pre-collisional particle-velocity fluctuation. For small values of R the stresses depend linearly upon the shear rate. At large values of R, both normal and shear stresses depend on the square of the shear rate. Furthermore Savage and Jeffrey (1981) estimated that a fluidized-bed subjected to a small shear should be an obvious example of small R, since Carlos & Richardson (1968) measured the velocity fluctuations in fluidized beds having essentially no mean motion and found the magnitude of v(r.m.s.) (root-mean-square pre-collisional particle-velocity fluctuation) to be a function of the fluidizing velocity. From the analysis by Savage & Jeffrey the viscosity coefficient of a fluidized-bed, at low shear rates, is

$$\eta=\frac{5}{6}\left(\frac{2}{\pi}\right)^{0.5}\nu g_0(\nu)\rho_s d v(r.m.s.) \tag{22}$$

where ν is the volume fraction of particles, $g_0(\nu)$ is the radial distribution function proposed by Carnahan and Starling(1969) and d is the particle diameter. The dependence of the viscosity coefficient upon the density for the fluidized-bed snow experiment is plotted in Fig. 41 together with the lines calculated by Eq. (22) for different v(r.m.s.). The lines are in a reasonable agreement with the trend of A, B and D except the two data points of A above $\rho=400$ kg/m^3 and C shows a large effect of d because the sample has a fairly wide distribution of d (Fig. 27). The magnitude of v(r.m.s.) in Fig. 41 chosen to fit the measured data ranges from 0.01 m/s to 0.05 m/s and seems to become smaller with increasing diameter from A to D. It is interesting to note that the magnitude of the fluctuation velocity is roughly one-tenth to one-hundredth of the upward air velocity (0.5 to 1 m/s).

In addition to the effect of the interstitial fluid (air), three mechanisms are recognized by which the stresses can be generated in a fluidized snow under shearing motion: (1) friction developed when particles are contact with neighbors; (2) transport of momentum by particle translation from one shear layer to another; and (3) momentum transport by particle collisions. Although all the three processes can coexist in certain flow regimes, usually one of them will play a predominant role. At high particle concentrations and low shear rates, particles are in close rubbing contact and inertia effects are small; the stresses are of the quasi-static, rate-independent, Coulomb-friction-type often described in soil mechanics literatures, e.g. for dry cohesionless granular materials like sand. At very low concentrations and high shear rates, we might expect the granular material to behave like a dilute gas; The mean free path is large compared with particle diameters and the shear stress may result from the interchange of particles between adjacent layers of material moving at different velocities. When both the concentrations and the shear rates are moderately high, the overall situation is analogous to a viscous liquid in which the exchange of momentum occurs primarily by the continuous action of molecular collisions.

The densities and shear rates of our experiments correspond to those of the third case in which the exchange of momentum is effected primarily by the particle collisions. This

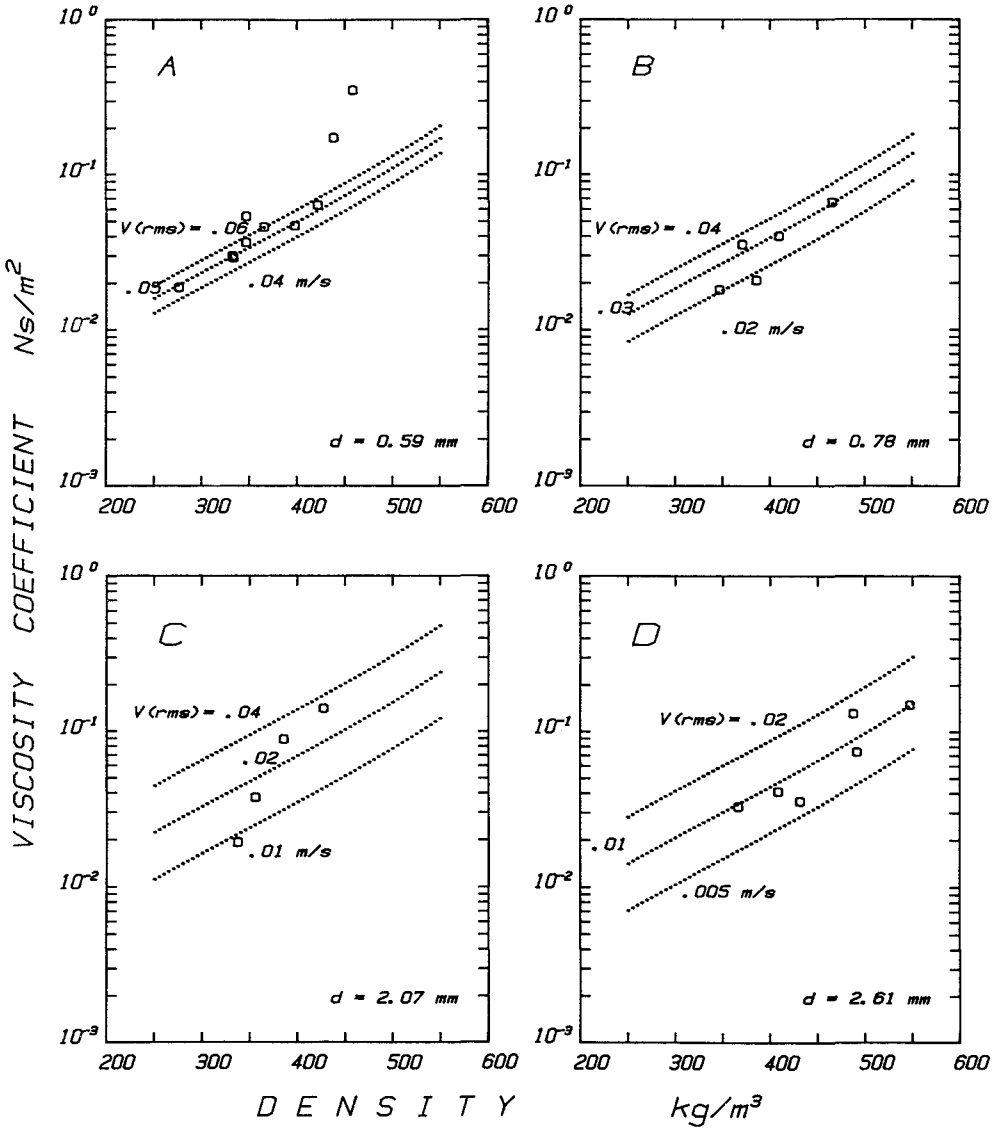

Fig. 41 Comparisons of the fluidized-bed experimental results with the calculated results. The dotted lines represent the theory of Savage & Jeffrey (1981).

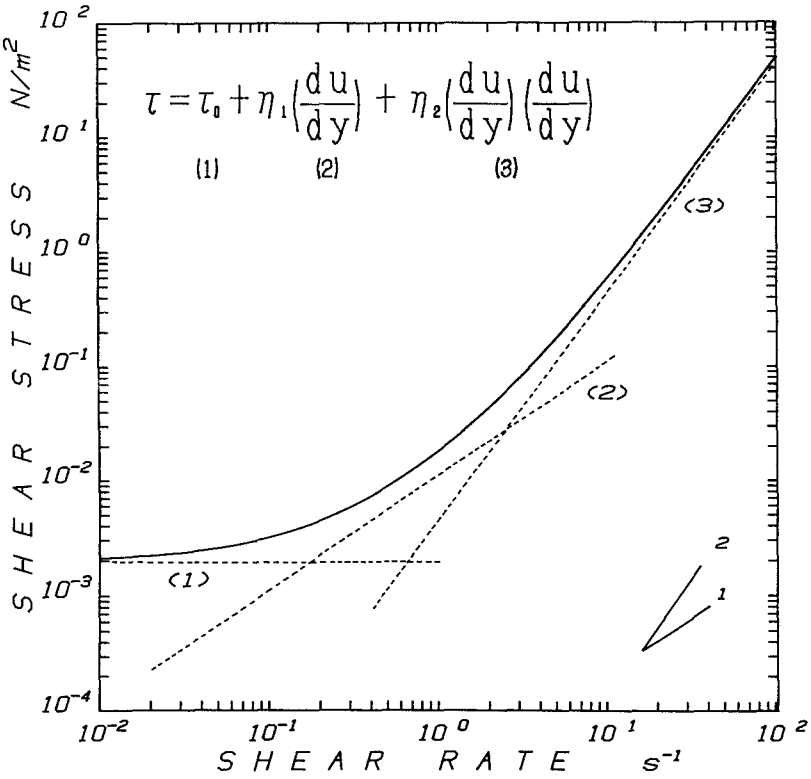

Fig. 42 Relation between the shear stress and the shear rate for the fluidized snow of 200 kg/m³. Dotted lines show the individual contributions of Eq. (23) and solid line shows the total shear stress.

category can be divided into two as suggested in Fig. 39: at lower shear rates shear stresses are linearly proportional to the shear rate; at higher shear rates shear stresses depend on the square of the shear rate. The mechanism which brings the difference is considered as follows; One explanation is a contribution of the interstitial fluid viscosity: although the interstitial fluid seems to play a minor role and the main contributions to the stresses could be attributed to particle collisions at the higher shear rates, fluid viscosity likely becomes important at lower shear rates. The other explanation is that the ratio of the mean shear velocity to the r.m.s. fluctuating velocity proposed by Savage and Jeffrey (1988) determines the relation between the shear stress and the shear rate.

It is reasonably concluded that all the effects mentioned above coexist although one of them may play a predominant role. Thus it is possible to represent the shear stress as a sum of three parts in general:

$$\tau=\tau_0+\eta\frac{du}{dy}+\eta_2\left(\frac{du}{dy}\right)^2 \tag{23}$$

where the first term is the dry friction part, the second is the viscous term, and the third is the quadratic viscous (turbulent) term. With reference to the experimental data for the fluidized snow of 200 kg/m^3 the values of each term in Eq. (23) were obtained. Fig. 42 shows not only the individual contribution but also the total shear stress. It is shown in this figure that the shear stress is roughly independent of the shear rate under 10^{-1} s^{-1}; above 20 s^{-1} the shear stress depends upon the square of the shear rate; in between the two regions the shear stress seems linearly proportional to the shear rate. Let us consider an example of a natural avalanche. Nishimura and others (1989) analyzed the impact force data of an avalanche and estimated a vertical velocity gradient, that is the shear rate of the avalanche flow, which was in a range 1 to 7 s^{-1}. Therefore it is concluded that when we discuss the dynamics of avalanches, not only the quadratic term but also a linear term, that is, the viscosity of the fluidized snow should be taken into account as suggested by Nishimura and Maeno (1989).

By studying the flow of neutrally buoyant wax spheres between concentric cylinders, Bagnold (1954) found three flow regimes depending upon a value of a dimensionless shear rate B, which was analogous to a conventional Reynolds number. The Bagnold number B is defined as the ratio of the inertial to the viscous forces:

$$B=\rho_s\lambda^{-1}\lambda^{0.5}d^2\frac{du}{dy}, \tag{24}$$

where ρ_s is the density of the granular material, d is the grain diameter, μ is the interstitial fluid viscosity, du/dy is the shear rate which in the case of linear velocity gradient is the velocity divided by the shear layer thickness, and λ is the linear concentration which is the ratio of the grain diameter to the mean free separation distance between grains given by

$$\lambda=\frac{1}{(\rho_0/\rho)^{1/3}-1}, \tag{25}$$

where ρ_0 is the bulk density at maximum mechanical packing; ρ is the bulk density in the shear layer. Bagnold found that for $B<40$, which corresponds to the low shear rate region, the flow is in the macroviscous regime. In this regime fluid viscosity is important, the stresses are linearly proportional to the shear rate. For $B>450$, which corresponds to the high shear rate region, it is in the grain-inertia regime. He believed that the interstitial fluid plays a minor role and that the main contributions to the stresses could be attributed to interparticle friction and collisions. In this region stresses depend on the square of the shear rate. He refers to the region between these two limits as the transition region where the effects of both fluid viscosity and grain inertia are important. For our snow experiment of diameter 0.59 mm shown in Fig. 39, the values of ρ_s, ρ_0, ρ_i are 910 kg/m^3, 550 kg/m^3 and 200 kg/m^3 respectively; the viscosity of air is 17.1×10^{-6} Ns/m^2 at 0 °C. Substitution of the above values into Eq. (24) showed that the region at shear rates lower than 1.1 s^{-1} corresponds to the viscous regime and that the higher rates than 16.8 s^{-1} to the grain-inertia regime. As

compared with Fig. 42, Bagnold's number criteria seems to be roughly applicable to determine the dynamical properties of the fluidized snow.

V.4. *Conclusions*

Comparing viscosity coefficients obtained in the inclined-chute experiment in Chapter III and the fluidized-bed experiment in Chapter IV, it became evident that shear stresses are linearly proportional to the shear rate in a lower shear rate region and shear stresses depend on the square of the shear rate in a higher shear rate region. In fact the constitutive equation of fluidized snow (Eq. (20)) was confirmed to represent the actual velocity profiles of snow flow; At high shear rates Eq. (20) can be applied to the fluidized snow. Referring above experimental results and considering the mechanism of momentum transport processes in fluidized snow, a constitutive equation which expresses the general dynamical properties of fluidized snow was derived as Eq. (23); Total shear stress is expressed as the sum of dry friction, viscous and quadratic viscous terms.

VI. Numerical simulations of avalanche dynamics

Many models have already been proposed to describe the motion of snow avalanches (Mellor 1978; Perla and others, 1980). In deriving the equations of avalanche motion the most important factor must be the resistance force exerted during the motion. The resistance force, R, acting on a snow avalanche has been traditionally expressed as a power series of velocity u (Salm, 1966):

$$R=A+Bu+Cu^2 \tag{26}$$

where A is a dry friction, B is a viscous friction resistance and C is a turbulent friction resistance. Dry friction, which is independent of the velocity, is the Coulomb force expressed as:

$$A=\mu N, \tag{27}$$

where μ is the dry friction coefficient and N is the normal force. The viscous resistance Bu can be expressed as:

$$Bu=\frac{\eta S}{\lambda}u \tag{28}$$

where η is the viscosity of fluidized snow and λ and S are the shear layer thickness and area respectively. The turbulent resistance (Cu^2) includes air drag and the plowing effect of snow, as well as the turbulent internal friction inside the avalanche. If we neglect the air drag and the plowing effect, Eq. (26) is just the same as Eq. (23) which represents the dynamical properties of fluidized snow. Although the viscous forces term (Bu) has been neglected in most earlier numerical simulations of snow avalanches (Mellor, 1978; Perla, 1980;

Nohguchi, 1983), our results discussed in Chapter V suggest this term should be taken into account in order to achieve a more realistic and physically reasonable simulation of snow avalanches. In this chapter we simulate numerically the motion of fluidized snow flow along the chute first and secondly this model is applied to artificial and also natural avalanches observed in the Shiai-dani region.

The avalanche model used here (Maeno and Nishimura 1987) treats the motion of a center-of-mass of an avalanche in a similar manner as Perla and others (1980) and Nohguchi (1983). The velocity and the running route of an avalanche is automatically computed at every point on a given real two or three-dimensional topography.

VI.1. Simulation of chute-flows

The equation of motion of a mass is given as:

$$M_0 \frac{du}{dt} = M_0 g \sin\theta - R, \tag{29}$$

where M_0 is the total mass of snow flow. As described before, the resistance force acting on snow flow R is

$$R = A + Bu + Cu^2 \tag{30}$$

where A is constant and other terms are described as follows:

$$B = \eta_1 \left(\frac{u}{\lambda}\right) S, \tag{31}$$

and

$$C = \eta_2 \left(\frac{u}{\lambda}\right)^2 S. \tag{32}$$

As discussed before, the chute flow experiment was a typical example of high shear rate. As shown in Fig. 42, the contribution of A (10^{-3} to 10^{-2} N/m^2) is negligibly small in a high shear rate region thus we put $A=0$ in this calculation. Assuming that the configuration of the snow flow is 6 m long, 0.08 m wide and 0.04 m high, the bottom surface area become $S=0.48$ m^2. It is assumed further that a velocity shear exists all over the depth of the flowing layer: thickness of shear layer λ was put 0.04 m. Since the average density of snow flow was around 200 kg/m^3, Fig. 21 and Fig. 38 give η_1 and η_2 as 1×10^{-2} Ns/m^2 and 4×10^{-3} Ns^2/m^2 respectively. The equation of motion was solved by a Runge-Kutta method. Although three effects (A, B and C) coexist, C played a predominant role in fact except for quite low velocity range. Fig. 43 shows the observed and calculated snow flow velocities along the inclined chute. Horizontal axis shows the distance from the entrance of the chute, which is different from x in Fig. 2 and here $x=0$ corresponds to 2.6 m in this figure. In addition to the data shown in Fig. 13, Fig. 43 gives some results obtained when a horizontal chute of 2 m long was joined to the inclined one. Since the sudden change of inclination gives the drastic change of snow flow behavior, experiments with the elongated chute were carried out

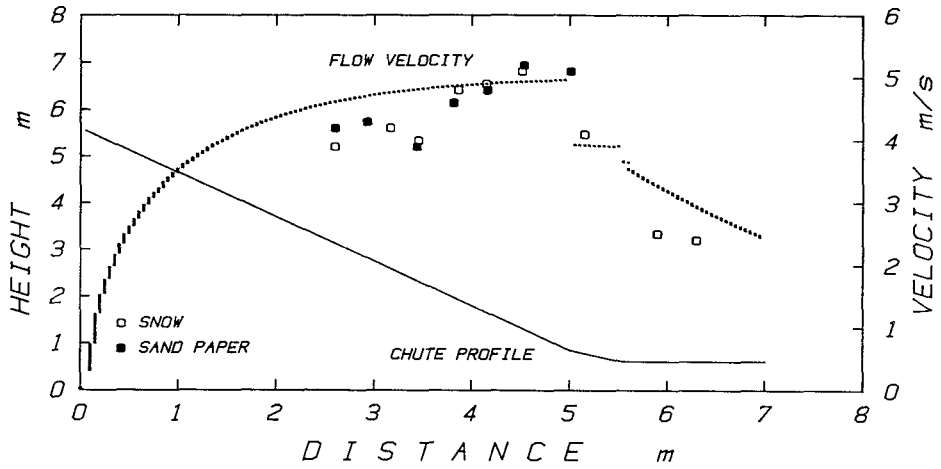

Fig. 43 Observed and calculated snow flow velocities along the inclined chute. Solid line shows the chute profile; Circles show the observed velocities (○ : snow floor, ● : sand paper floor); Dotted line represents the calculated velocity.

only for the snow floor as shown in Fig. 43. It is evident that calculated velocity along the 7 m long chute agrees with the observed results within the accuracy of ±20 %.

VI.2. *Simulations of Shiai-dani avalanches*

In the Shiai-dani region, whose approximate length and angle of inclination are respectively 2000 m and 33 degrees, an experimental project of snow avalanche is under way (Kawada and others, 1989). In this project we have intended to make systematic investigations including visual observations of both artificial and natural avalanches.

On February 1st, 1987 an avalanche was initiated by dynamiting large amounts of snow cornices at the Shiai-dani ridge. The artificially released avalanche (about 6.3×10^5 kg) ran down a distance of about 1 km down the slope in about 50 s, but did not reach the observation site where we mounted many measuring devices on two 5 m high mounds. Fig. 44 shows the cross-section of the avalanche slope and the front velocity estimated at the central part of the avalanche. The front velocity varied within the range 10-50 m/s; this variation was thought to have been caused by the irregular snow topography.

Next during a heavy snow storm on Feb. 3rd in 1988, a powder-snow avalanche broke out and came across the observation site. Internal velocity obtained from a combination of the lag time that gave the highest correlation and the distance between the two measuring points was 25 to 35 m/s. More detailed method and analyses of the data are given in Nishimura and others (1989).

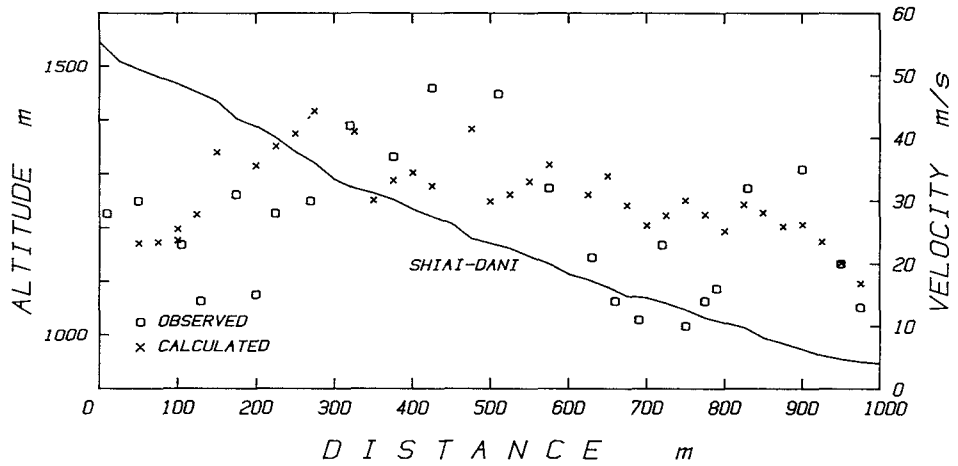

Fig. 44 Observed and calculated avalanche velocities. The avalanche was released artificially on February 1, 1988 at Shiai-dani. Open circles show the velocities of the avalanche front estimated from the video film; Crosses represent calculated avalanche velocity; Solid line is a cross section along the avalanche shoot.

We simulate the time variation of these avalanche movements numerically in the following. The avalanche model used is the same in principle used in the previous section; but A in Eq. (30), which is usually considered not to depend on the velocity, was assumed to decrease with velocity. Although this term was neglected in the chute flow calculation, actual avalanches are usually set in motion with the release of a cohesive slab; the thickness more than 1 m is not unusual (Perla, 1980). Further even in the natural stage the avalanche was found to be composed of many blocks embedded in fluidized snow (Nishimura and others, 1989). Thus dry friction is considered to be larger than the values obtained from fluidized snow experiment (10^{-2} N/m^2) and depend on the avalanche velocity. We assumed A as follows:

$$A=\mu N=(\mu_\infty+(\mu_0-\mu_\infty)\exp(-u/V\ ))N, \tag{33}$$

where μ_0 and μ_∞ are respectively the friction coefficients at velocities of zero and infinity and V is a constant. In the following calculation figures of $\mu_0=0.5$, $\mu_\infty=0.1$ were used. Though Maeno and Nishimura's numerical model also took into account the effect of snow entrainment, it was ignored in this calculation.

Although the available information about the internal structure of avalanche is very limited, the internal density of the avalanche on 3 and 23 Feb. 1978 in the Shiai-dani region was calculated as 50 to 300 kg/m^3 (Nishimura and others, 1987, Nishimura and others, 1989)

on the assumption that this avalanche was composed of fluidized snow and dense snow blocks. Thus, using data shown in Fig. 42, η_1 in Eq. (32) is estimated as ranging from 10^{-4} Ns/m^2 to 10^{-2} Ns/m^2; in Fig. 50 η_2 in Eq. (33) is from 10^{-5} Ns^2/m^2. In the following calculations, we use values of 10^2 kg/s as B, 80 kg/m as C, $S=5\times10^3$m^2, $\lambda=0.5$ m, $\rho=200$ kg/m^3. It should be noted that the turbulence-coefficient, C, was set as 80 kg/m, which is very much smaller than the values frequently used. To take into account the effect of temperature rise due to sunshine(-3.5 °C), V was put to be 50 m/s in the simulation of the artificial avalanche.

The calculated avalanche velocities are shown in Fig. 44. Calculated velocities roughly agree with the measured velocities, in particular for the last 100 m where the velocity decreased rapidly and came to stop. But it is seen that the simulation does not always follow the velocity change along the valley. We can consider that the largest cause for the discrepancy is the profile of Shiai-dani. The profile used in this calculation is the one in summer when the valley is not covered with snow, whereas the profile in winter showed the irregular snow topography due to much debris formed by frequent smaller avalanches from steep side slopes of the valley.

Fig. 46 shows the typical avalanche path calculated on the three-dimensional topography of Shiai-dani. Values of parameters used in the calculation are the same as in Fig. 44 except that V is 30 m/s. The unit mesh is 25 m, and the position of the center of mass of avalanche is given as a circle every 2 s. Fig. 45 shows the change in velocity along the avalanche shoot

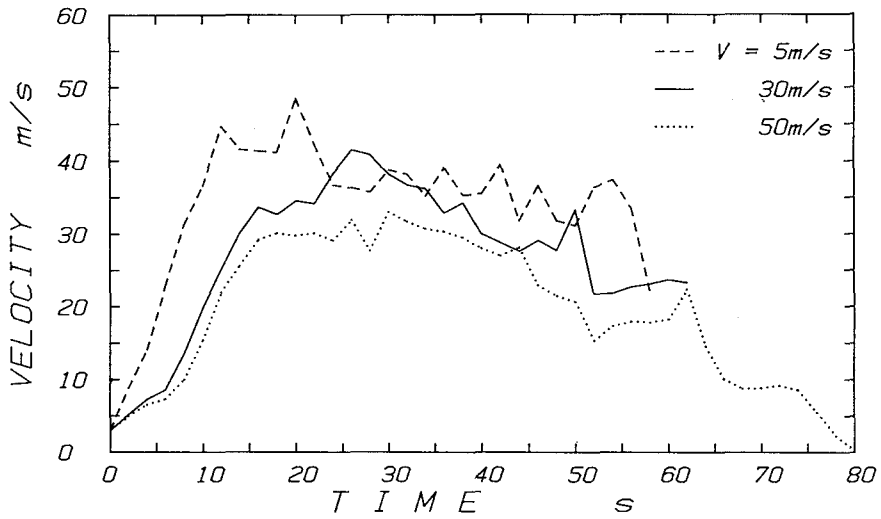

Fig. 45 Numerical simulations of the natural snow avalanche motions in the Shiai-dani region on February 3, 1988. Values of parameters selected are the same as in Fig. 44 but V in Eq. (23).

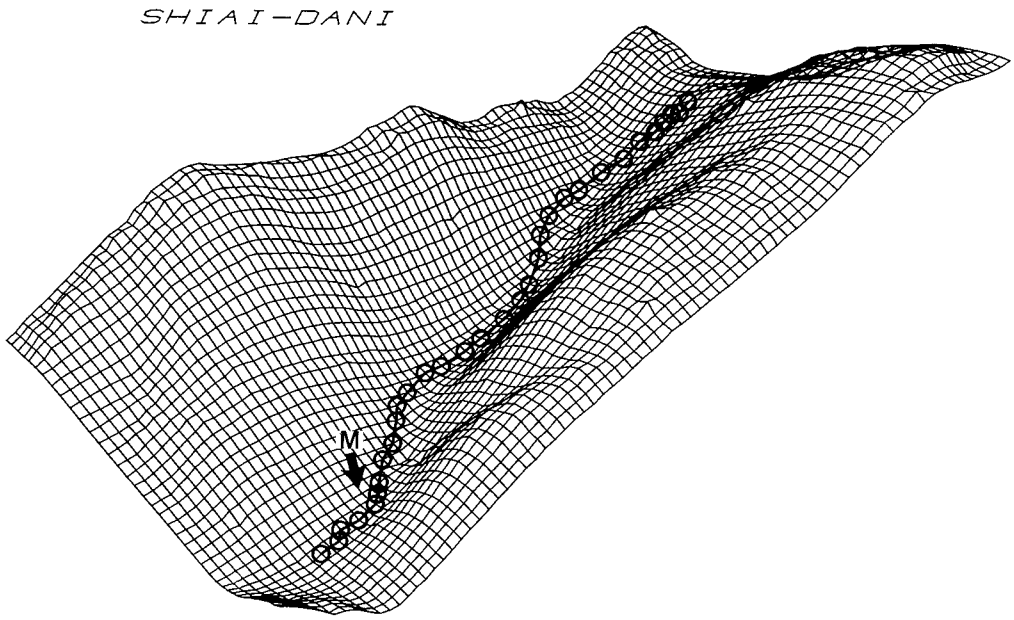

Fig. 46 Change in calculated velocities of snow avalanche along the avalanche shoot. *M* represents the observation site.

and the broken, solid and dotted lines are results obtained for V =5 m/s, 30 m/s, 50 m/s respectively. Since the avalanche velocity at the observation site, *M* (Fig. 46) has been calculated to be 25−35 m/s, the solid line, that is the line for V =30 m/s, is considered the best to simulate the actual avalanche on Feb. 3 1989.

From the discussions described above, we can conclude that the run-out distance depends on A strongly: artificial avalanche, which is in the case of large A, was released under a high temperature condition (−3.7 °C) and ran down only 1 km; natural avalanche, which is for small A, broke out at lower temperature (−15 °C) and ran down over 2 km and came across the observation site. It is reasonable that A becomes larger at higher temperatures because the friction between snow and snow increases with increasing temperature (Casassa, 1989); since fluidization of snow becomes harder at higher temperatures many lager snow blocks and slabs must be embedded in the avalanche (Nishimura and Maeno, 1978). But both the values of B and C may also depend on the temperature near the melting point of ice, as was discussed in the previous chapter. Furthermore we have ignored the effect of the entrainment of snow. This assumption seems reasonable in case of the artificial avalanche since the recorded video-films showed the total volume of the avalanche did not change much. But generally the assumption is not correct for most avalanches.

VI.3. *Conclusions*

Substituting the experimental results obtained in Chapters III, IV and V into Eq. (26) which is equivalent to Eq. (23), we simulated numerically the motions of fluidized snow flow along the chute. Furthermore this model was applied to artificial and natural avalanches observed in the Shiai-dani region. Not only the quadratic term (turbulent term) but also a linear term, that is, the viscosity of the fluidized snow was taken into account as suggested in Chapter V. Calculated velocities along the chute (Fig. 43) and the avalanche shoot (Fig. 44) agreed well with the observed results. Effects of dry friction term A was also discussed in case of avalanche simulations.

VII. Concluding remarks

Experiments with an inclined chute system and a fluidized snow bed were carried out in a cold laboratory in order to investigate the mechanical properties of fluidized snow. The results are summarized as followings:

1) In the steady-state part of the snow flow, velocity profiles and bulk densities were obtained with the high-speed video system and the drag meter. Bulk densities were assumed to be uniform with depth and Eq. (7) was applied to simulate the obtained velocity profiles. The apparent viscosity coefficients obtained ranged from 8.3×10^{-2} to 4.5×10^{-1} Ns/m^2 and τ_0 from 0 to 10 N/m^2 for the bulk densities of 100 to 200 kg/m^3 and the shear rate of 60 to 70 s^{-1}.

2) Fluidized-bed experiment of snow showed that the fluidized snow behaves like a Bingham body for the shear rate of 1 to 15 s^{-1}. Viscosity coefficients and yield stresses were from 10^{-2} to 10^{-1} Ns/m^2 and 0 to 10^{-2} N/m^2 respectively. It was found that the viscosity increased rapidly with the bulk density.

3) Comparing the viscosity coefficients obtained above (1) and 2)) in special reference to the shear rate of each experiment and re-examining the assumptions made, it was found that shear stresses are linearly proportional to the shear rate in a lower shear rate region and shear stresses depend on the square of the shear rate in a higher shear rate region. Eq. (20) was found to represent the actual snow flow velocity profiles. Furthermore a constitutive equation which expresses the general dynamical properties of fluidized snow was derived as Eq. (23); Total shear stresses are expressed as the sum of the dry friction part, the viscous term and the quadratic viscous term (turbulent term).

4) The dynamical properties of the fluidized snow obtained above were applied to the numerical simulations of not only the fluidized snow flow motion along the chute but also artificial and natural avalanches in the Shiai-dani region. The model showed a good fit to observed data.

The effect of temperature on the viscosity of fluidized snow does not seem important

(Figs. 29 and 30), but the effect on τ_0, and η_2 might become predominant at much higher temperatures near the melting point of ice because of the increasing adhesion between snow particles. Maeno and Nishimura (1979) found that stable uniform fluidization with the fluidized-bed system could not be generated in snow composed of dendrite crystals or ice particles of diameter roughly less than 0.3 mm due to increased coagulation between these fine complex-shaped ice particles. Therefore effects of size and shape might be also important on the dynamical properties of fluidized snow. More detailed understanding of fluidized snow behavior, such as the effects of temperature, shape and size of snow particles etc., are a subject to be solved in future.

Acknowledgments

The author would like to acknowledge the continuing kind guidance and encouragement of Prof. N. Maeno of the Institute of Low Temperature Science, Hokkaido University. The author is also grateful to Prof. G. Wakahama of the Institute of Low Temperature Science, Prof. T. Tanaka of Department of Chemical Process Engineering and Prof. K. Nakao of Department Geophysics, Hokkaido University for their helpful comments and discussions. The considerable assistance in the investigations and several helpful discussions with Dr. R. Naruse and Dr. H. Narita of the Institute of Low Temperature Science are gratefully acknowledged. He is indebted to graduated students Mr. S. Murakami, Mr. K. Kosugi and Mr. G. Casassa for their helpful cooperation in the experiments. All this work would not have been possible without the help of the workshop of our institute who made all the experimental equipments.

References

Bagnold, R.A., 1954. Experiments on a gravity-free dispersion of large solid spheres in a Newtonian fluid under shear. *Proc. Roy. Soc. London, Ser.* **A**, **225**, 49–63.

Bucher, E. and Roch, A., 1946. Reibungs und Packungswider stande bei raschen Schneebeweguagen. Report, Eidg. Inst. fur Schnee und Lawinenforsch, Davos-Weissfluhjoch, Switzerland, 9pp.

Carahan, N. F. and Starling, K. E., 1969. Equations of state for non-attracting rigid spheres, *J. Chem. Phys.*, **51** 635–636.

Carlos, C. R. & Richardson, J. F. 1968. Solids movement in liquid fluidized beds. I. Particle velocity distribution. *Chem. Engng Sci.* **23**, 813–824.

Casassa, G., Narita, H. and Maeno, N. 1989. Measurements of friction coefficients of snow blocks, *Annals of Glaciology*, **13**, 40–44.

Casassa, G. 1989. Studies on snow-to-snow friction. Master thesis, Department of Geophysics, Faculty of science, Hokkaido university.

Dent, J. D. and Lang, T. E. 1983. A biviscous modified Bingham model of snow avalanche motion. *Annals of Glaciology*, **4**, 42–46.

Goodman, M. A. and Cowin, S. C. 1971. Two problems in gravity flow of granular materials, *J. Fluid. Mech.*, **45**, 321–339.

Hanes, D. M. and Inman, D. L. 1985. Observations of rapidly flowing granular-fluid materials, *J. Fluid Mech.*, **150**, 357−380.

Hunger, O. and Morgenstern, N. R. 1984. High velocity ring shear tests on sand, *Geotechnique* **34**, No. 3, 415−421.

Ishida, M. and Hatano, H. 1983. The flow of solid particles in an aerated inclined channel, in Advances in the mechanics and the flow of granular materials, vol. 2, Shashinpoor, M. ed., 565−575.

Jenkins, J. T. and Savage, S. B. 1983. A theory for the rapid flow of identical, smooth, nearly elastic spherical particles. *J. Fluid Mech.* **130**, 197−202.

Kobayashi, S. 1978. A consideration on mechanism of formation of transverse snow-waves, *Seppyo*, Vol. **40** (1), 22−30 (in Japanese).

Lang, T. E. and Dent, J. D. 1983. Basal surface-layer properties in flowing snow. *Annals of Glaciology*, **4**, 158−162.

Lang, T.E. and Dent, J. D., 1983. Basal surface-layer properties in flowing snow. *Annals of Glaciology*, **4**, 158−162.

Maeno, N. and Nishimura, K., 1978. Studies of Fluidized Snow. 1. Formation of Fluidized Snow and Its General Properties. *Low Tem. Sci., Ser.* **A**, **36**. 77−92 (in Japanese with English summary).

Maeno, N., 1986. Time variations of the density of mixed-phase snow flows as measured by an electric capacitance method. *Low Temp. Sci., Ser.* **A 45**, 19−26 (in Japanese with English Summary).

Maeno, N., Nishimura, K. and Kaneda, Y., 1980. Viscosity and heat transfer in fluidized snow, *J. Glaciol.*, **26**(94), 263−274.

Maeno, N. and Nishimura, K., 1987. Numerical computation of snow avalanche motion in a three-dimensional topography, *Low Temp. Sci., Ser.* **A**, **46**, 99−110 (in Japanese with English summary).

Mellor, M., 1975. A review of basic snow mechanics, *IAHS-AISH Publ.*, **114**, 251−291.

Mellor, M., 1978. Dynamics of snow avalanches. Rockslides and Avalanches (B. Voight and others eds.), Vol. 1, Elsevier, Amsterdam, 753−792.

Nakamura, T., Nakamura, H., Abe, O., Sato, A. and Numano, N. 1987. A newly designed chute for snow avalanche experiments, *IAHS-AISH Publ.* **162**, 441−451.

Nishimura, K. and Maeno, N., 1978. Studies of Fluidized Snow. 2. Viscosity and Heat Transfer Coefficients of Fluidized Snow. *Low Temp. Sci., Ser.* **A**, **36**. 93−102 (in Japanese with English summary).

Nishimura, K., Maeno, N. and Kawada, K. 1987. Internal structures of large-scale avalanches revealed by a frequency analysis of impact forces. *Low Temp. Sci., Ser.* **A**, **46**. 91−98 (in Japanese with English summary).

Nishimura, K. and Maeno, N. 1987. Experiments on snow-avalanche dynamics. Avalanche Formation, Movement and Effects (Proc. Davos Symp., Sept. 1986), *IAHS-AISH Pub.*, **162**, 395−404.

Nishimura, K. and Maeno, N. 1989. Contribution of viscous force to the avalanche dynamics. *Annals of Glaciology*, **13**. 202−206.

Nishimura, K., Narita, H., and Maeno, N. 1989. Internal structures of Powder-snow avalanches. *Annals of Glaciology*, **13**. 207−210.

Nohguchi, Y. 1983. Traveling path of snow avalanche on model configuration. *The report of the National Research Center for Disaster prevention*, **31**, 153−174.

Perla, R., Cheng, T. T. and McClung, D. M. 1980. A two parameter model of snow avalanche motion, *J.* of *Glaciol.*, **26**, 94, 197−207.

Perla, R. 1980. Avalanche release, motion and impact. Dynamics of Snow and Ice Masses (S. C. Colbeck ed.), Academic Press. 397–462.

Prandtl, L. 1965. Fuher durch die Stromungslehre, Friedr. Vieweg & Sohn, Braunschweig.

Salm, B. 1966. Contribution to avalanche dynamics, *IAHS-AISH Publ.*, **69**, 182–195.

Savage, S. B. 1979. Gravity flow of cohesionless granular materials in chutes and channels, *J. Fluid Mech.*, **92**(1) 53–96.

Savage, S. B. and Jeffrey D. J. 1981. The stress tensor in a granular flow at high shear rates., *J. Fluid Mech.*, **110**, 255–272.

Savage. S. B. 1983. Granular flows down rough inclines-Review and extension. Mechanics of Granular Materials: New Models and Constitutive Relations, (J. T. Jenkins and M. Satake eds.) Elsevier Science Publishers B. V., Amsterdam.

Savage, S. B. and Mckeon, S. 1983. Shear stresses developed during rapid shear of concentrated suspensions of large spherical particles between concentric cylinders, *J. Fluid Mech.*, **127**, 453–472.

Savage, S. B. and Sayed, M. 1984. Stresses developed by dry cohesionless granular materials sheared in an annular shear cell, *J. Fluid Mech.*, **142**, 391–430.

Suzuki, A. and Tanaka, T. 1971. Measurement of flow properties of powders along an inclined plane. *Ind. Engng. Chem. Fundam*, **10**, 84–91.

Takahashi, K. 1937. On the dynamical properties of Granular Mass. Geophys., **11**, 165–175.

Takahashi, T. 1980. Debris flow on prismatic open channel. J. Hydraulic Division, *ASCE*, **106**, NO. hy3, 381–396.

Voellmy, A. 1955. Uber die Zertsorungskraft von Lawinen, Schweizerische Bauzeitung, Jahrg. 73, S. 159–162, 212–217, 246–249, 280–285.